

18. SITE 942¹

Shipboard Scientific Party²

HOLE 942A

Date occupied: 9 May 1994
Date departed: 10 May 1994
Time on hole: 1 day, 5 hr, 15 min
Position: 5°44.546'N, 49°5.464'W
Bottom felt (drill pipe measurement from rig floor, m): 3357.7
Distance between rig floor and sea level (m): 11.40
Water depth (drill pipe measurement from sea level, m): 3346.3
Penetration (m): 177.60
Number of cores (including cores having no recovery): 20
Total length of cored section (m): 177.60
Total core recovered (m): 152.60
Core recovery (%): 85
Oldest sediment cored:
Depth (mbsf): 177.60
Nature: Silty clay
Earliest age: Pleistocene

HOLE 942B

Date occupied: 10 May 1994
Date departed: 10 May 1994
Time on hole: 6 hr, 45 min
Position: 5°44.557'N, 49°5.460'W
Bottom felt (drill pipe measurement from rig floor, m): 3357.1
Distance between rig floor and sea level (m): 11.40
Water depth (drill pipe measurement from sea level, m): 3345.7
Penetration (m): 74.00
Number of cores (including cores having no recovery): 8
Total length of cored section (m): 74.00
Total core recovered (m): 56.91
Core recovery (%): 76
Oldest sediment cored:
Depth (mbsf): 74.00
Nature: Silty clay
Earliest age: Pleistocene

HOLE 942C

Date occupied: 10 May 1994
Date departed: 11 May 1994
Time on hole: 12 hr
Position: 5°44.552'N, 49°5.452'W
Bottom felt (drill pipe measurement from rig floor, m): 3360.2
Distance between rig floor and sea level (m): 11.40
Water depth (drill pipe measurement from sea level, m): 3348.8
Penetration (m): 71.50
Number of cores (including cores having no recovery): 5
Total length of cored section (m): 42.30
Total core recovered (m): 44.03
Core recovery (%): 104
Oldest sediment cored:
Depth (mbsf): 42.30
Nature: Silty clay
Earliest age: Pleistocene

Principal results: Site 942 (proposed Site AF-20) is located on the crest of an abandoned levee to the west of the main part of the Amazon Fan. It was intended to provide a hemipelagic reference section on the western side of the fan to study equatorial Atlantic paleoclimate and paleocirculation patterns. A secondary objective of the site was to date and characterize the sediment source of the underlying levee.

The site was selected from a *Conrad* seismic-reflection profile (C1612; 1925UTC on 26 July). The precise position was determined from a pre-site echosounder profile from the *JOIDES Resolution*.

Hole 942A was cored by APC to 104.0 mbsf, then by XCB to 177.6 mbsf, with total hole recovery of 152.6 m (85.9%). Hole 942B was cored to 74.0 mbsf and recovered 56.91 m (76.9%). Hole 942C was cored to 71.5 mbsf, with the exception of 13.8–36.0 and 55.0–62.0 mbsf, which were drilled without coring. Total recovery was 44.03 m (104.1%). Correlation of lithology and magnetic susceptibility shows that measured depths below seafloor in Hole 942C below Core 1H are about 4 m shallower than the corresponding depths in Holes 942A and 942B. This offset is attributed to a coring problem: the sediment is flat-lying.

Temperature measurements made at 51 and 80 mbsf (ADARA) show a mean geothermal gradient of 38°C/km. There was gas expansion in many cores. Methane was found throughout the hole, but higher hydrocarbons were not detected.

Six lithologic units are recognized, using Hole 942A as a type section:

Unit I (0–0.66 mbsf) is a bioturbated Holocene foraminifer-nannofossil clay, with a diagenetic iron-rich crust at its base.

Unit II (0.66–28.10 mbsf) consists of mud with interbedded laminae and beds of silt and very fine sand. The mud has 1.4%–4.5% carbonate content. The unit is subdivided into two subunits. Subunit IIA (0.66–23.85 mbsf) comprises bioturbated mud with hydrotroilite-stained mottles. It includes one sand bed at 14 mbsf. Rare laminae and thin beds of silt occur below 17 mbsf. Subunit IIB (23.85–28.10 mbsf) is composed of mud with

¹Flood, R.D., Piper, D.J.W., Klaus, A., et al., 1995. *Proc. ODP, Init. Repts.*, 155: College Station, TX (Ocean Drilling Program).

²Shipboard Scientific Party is as given in the list of participants in the contents.

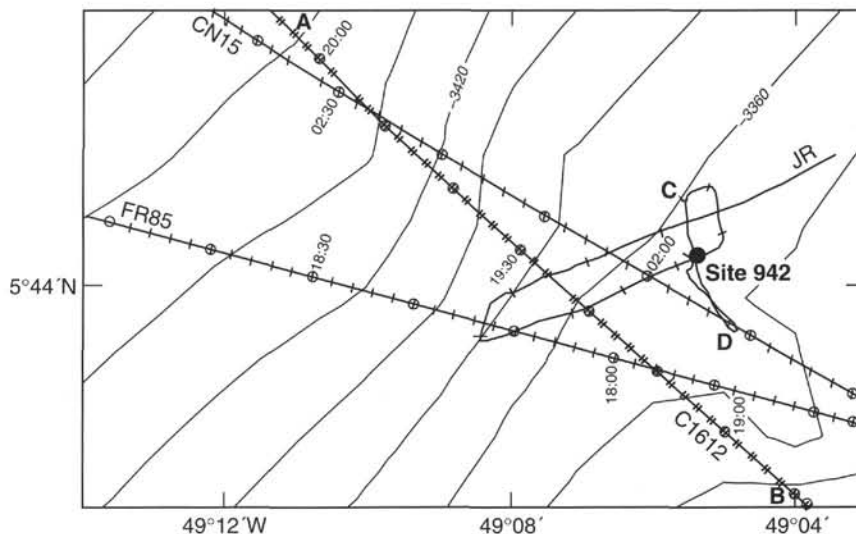


Figure 1. Location of Site 942 showing location of previous seismic profiles and the *JOIDES Resolution* ship track. Seismic profile A–B is shown in Figure 2; 3.5-kHz profile C–D is shown in Figure 3. Bathymetry in corrected meters.

thin to thick beds of silt and fine sand, which increase in frequency and thickness toward the base of the subunit.

Unit III (28.10–40.18 mbsf) comprises a thin calcareous mud resting on a sequence of mud with interbedded silt and sand. Subunit IIIA (28.10–28.80 mbsf) is a foraminifer-nannofossil-rich silty clay, with 14% carbonate. It has a gradational contact with the underlying subunit. Subunit IIIB (28.80–40.18 mbsf) consists of bioturbated mud, mottled with hydrotroilite, with interbedded laminae and beds of silt and sand. Silt and sand beds are particularly abundant from 36 to 40 mbsf. *Spreiten* burrows (probably *Echinocardium*) commonly disrupt the tops of sand beds.

Unit IV (40.18–65.20 mbsf) resembles Unit III, comprising a thin calcareous mud resting on a sequence of mud with interbedded silt and sand. Sand is more abundant than in Unit III. Subunit IVA (40.18–40.80 mbsf) is a foraminifer-nannofossil-rich clay similar to that in Subunit IIIA and with a gradational lower boundary. Subunit IVB (40.80–65.20 mbsf) consists of moderately burrowed dark greenish gray mud, alternating with beds and laminae of very fine sand and coarse silt, many of which are cross-laminated. Ripple-migration directions, determined on oriented cores, are to the north. The abundance of ripple lamination at this site probably reflects the abundance of very fine sand, compared with the dominance of silt at previous Amazon Fan sites.

Unit V (65.20–66.07 mbsf) consists of greenish-gray foraminifer-nannofossil clay with as much as 31% carbonate and gradational boundaries.

Unit VI (66.07–171.28 mbsf) consists of gray mud with laminae and rare beds of silt. Color banding and mottling are common. Carbonate content is generally 0.7%–4%. Two light-colored muds at the tops of turbidite beds with 14%–17% carbonate contain diagenetic siderite.

Foraminifers and nannofossils are common to abundant in Units I–V and the upper part of Unit VI, but are rare in the lower part of Unit VI. The *P. obliquiloculata* 40-ka datum is found at 23.03 mbsf. Units III, IV, and V (28.1–66.0 m) contain nannofossils of Zone CN15a (85–260 ka). *G. tumida* is absent below 70.38 mbsf; this lower interval is interpreted as the W zone (isotopic Stage 6, >130 ka).

Two geomagnetic excursions are represented by short intervals of anomalous remanence direction and intensity. The Lake Mungo Excursion (30 ka) occurs at 11.5 mbsf in Hole 942A, but was not detected in Hole 942B. The second, at 41.5 mbsf in Hole 942B (also found in Hole 942C), correlates to the Blake Event (105 ka). Short wavelength (about 0.5 m) oscillations in magnetic inclination, interpreted as secular variation, were detected between 1 and 15 mbsf. Remanence intensity variation can be correlated between holes.

Index properties in Units II–V show more scatter than samples at similar depths at previous Leg 155 sites. Some samples at the base of Unit IV and the top of Unit VI have anomalously high grain density (2.8–2.9 g/cm³).

Total organic-carbon content is generally 0.4%–0.8% in Units I–V, but then gradually increases to >1.0% in the lower part of Unit VI. Elevated sulfur content occurs immediately below Units I and V. In pore-water samples, calcium, magnesium, alkalinity, and salinity are low in the interval from 30 to 100 mbsf.

This site provides a reference section for biostratigraphy and stable isotopes on the western side of the Amazon Fan. The three carbonate-rich intervals (Subunits IIIA and IVA and Unit V) are interpreted to correspond to isotopic Stages 5a, 5c, and 5e, with the Blake paleomagnetic event in Stage 5c and the greatest abundance of microfossils when sea level was highest in Stage 5e. The overall sedimentation rate in Stage 5 is estimated to be 0.8 m/k.y. Turbidites in Subunits IIB through IVB (isotopic Stages 3–5) contain a high proportion of fine sand to silt and may be compositionally distinct from Amazon Fan levee turbidites: these sandy turbidites may be derived from a source north of the mouth of the Amazon River. The silty turbidites of Unit VI (isotopic Stage 6) appear to have the same provenance as Amazon Fan sediment.

SETTING AND OBJECTIVES

Introduction

Site 942 (proposed Site AF-20), located on the crest of an abandoned levee to the west of the major portion of the Amazon Fan, was intended to provide a hemipelagic reference section on the western side of the fan. This hemipelagic section will be compared to similar sections recovered at Sites 932, 937, and 938 on the central and eastern portions of the fan to study equatorial Atlantic paleoclimate and paleocirculation patterns. A secondary objective of the site was to sample the sediment of the underlying levee to determine the source of its sediment and the period during which the levee was active. This is the most westerly site drilled during Leg 155.

Setting

Site 942 is located on the crest of an abandoned levee to the west of the Amazon Fan (Fig. 1). GLORIA side-scan sonar, and seismic and sub-bottom profiles show that this channel-levee system is a positive-relief feature that rises above one or more debris-flow deposits (Figs. 2 through 4; Damuth et al., 1988). This elevated levee is a potential site on which hemipelagic sediment can accumulate with minimal reworking. Present seismic-reflection data are inadequate to correlate this channel-levee system with those sampled at other sites on the Amazon Fan. The channel may have received sediment from

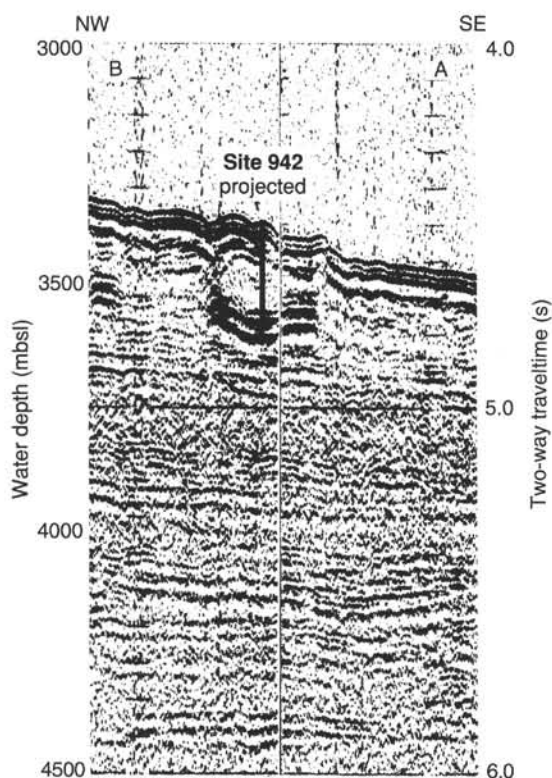


Figure 2. Seismic profile A-B near Site 942 (Conrad).

a different canyon, perhaps associated with drainage from the North Brazil (Amapa) coast.

The site was selected on *Conrad* air-gun profile (C2612, 1925UTC [1625 hr on profile] 26 July 1973; Fig. 2) and on a nearby *Farnella* air-gun profile (1810UTC on 15 Jan. 1982). *JOIDES Resolution* 3.5-kHz profiles show that Site 942 is near an abandoned channel (Fig. 3). The levee crest and channel are covered with at least 70 ms (53 m) of conformable, acoustically stratified sediment, suggesting that the channel has not been active for some period of time. A wedge of debris-flow material is intercalated in the sediment about

400 m southeast of Site 942 at about 15 mbsf (Fig. 3). This debris flow is apparently part of the Western Debris Flow of Damuth et al. (1988; the Central Debris Flow of Damuth and Embley, 1981), although its source upslope is uncertain. Sediment to the east of the debris-flow deposit does not appear disturbed in 3.5-kHz profiles except perhaps in a 4-m-thick zone from about 10 to 14 mbsf. Acoustically stratified sediment has been deposited beside and on top of the debris-flow deposit; sediment on top of the debris-flow deposit shows discontinuous reflections, perhaps because of the underlying topography. The 3.5-kHz profiles do not penetrate into the levee-crest sediment. The available seismic lines do not clearly show the depth of the buried levee crest.

Objectives

The principal objectives at Site 942 were:

1. To sample the anticipated hemipelagic stratigraphic section above the levee on the western side of the fan to determine past changes in ocean circulation and to aid in determining the stratigraphy of the fan sediment.
2. To sample the sediment of the underlying levee system to characterize its sediment and to determine its age and origin.

OPERATIONS

Transit: Site 941 to Site 942 (AF-20)

The 68-nmi transit from Site 941 to Site 942 took 6.1 hr. We conducted a short, 3.5-kHz PDR survey to locate the site. At 0725 hr 9 May, we deployed a beacon at 5°44.552'N, 49°5.470'W.

Hole 942A

We positioned the bit at 3352.0 mbrf and spudded Hole 942A at 1500 hr 9 May. Core 1H recovered 3.78 m, and the mud line was defined to be at 3357.7 mbrf. The distance from sea level to rig floor, which depends on the ship's draft, was 11.38 m for Holes 942A, 942B, and 942C. Cores 1H through 12H were taken from 3357.7 to 3461.7 mbrf (0–104.0 mbsf; Table 1) and recovered 104.96 m (100.9%). Cores 3H through 12H were oriented with the Tensor tool, and ADARA heat-flow measurements were made during Cores 6H

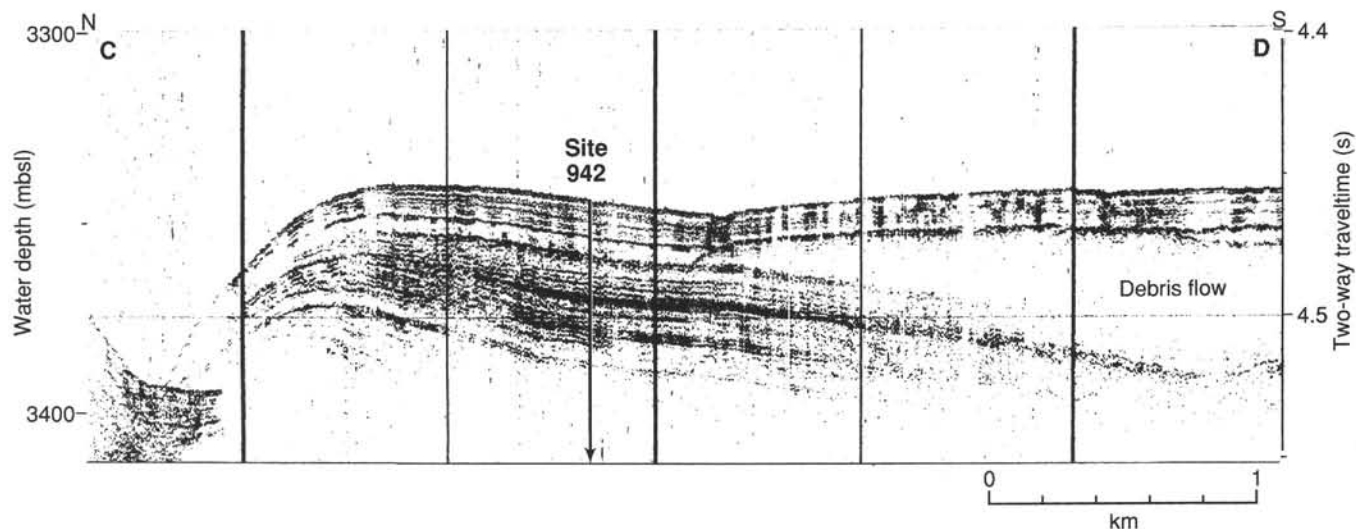


Figure 3. A 3.5-kHz profile at Site 942 (Profile C-D; *JOIDES Resolution*).

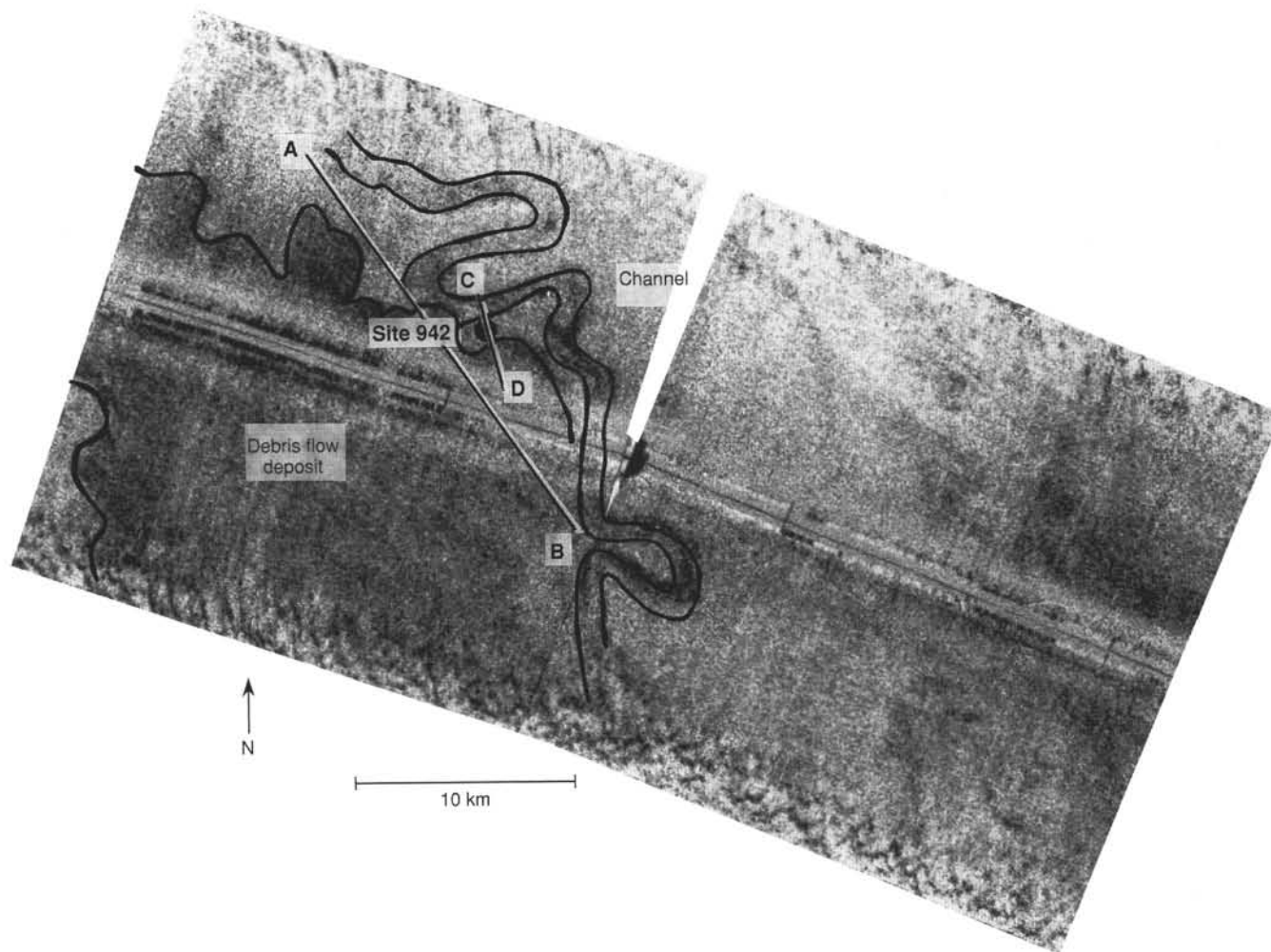


Figure 4. GLORIA side-scan sonar record showing the relationship of Site 942 to mapped channels and debris-flow deposits.

and 9H. Parts of Cores 5H, 9H, 11H, and 12H were disturbed as a result of either gas-induced extrusion of core from the liner onto the rig floor or collapsed core liners. During retrieval of the core barrel from the sediment on Cores 9H, 10H, 11H, and 12H, the overpull was 20,000 to 40,000 lb: the core barrel only partially stroked on the last two.

XCB Cores 13X through 20X were taken from 3461.7 to 3535.3 mbrf (104.0–177.6 mbsf), coring 73.6 m and recovering 47.69 m (64.8%). The overall APC/XCB recovery was 86.0%.

We tested the XCB flow control valve (FCV) at this site. Four cores were obtained with the FCV and four without it. The four runs with flow control cored 34.9 m and recovered 25.56 m (73%), and the four runs without flow control cored 38.7 m and recovered 22.13 m (57%). Operating parameters were 10,000 lb wob at 80 rpm with 100 amp torque, circulating 25 gpm at 125–150 psi. When we retrieved the bit after coring two additional holes (Holes 942B and 942C), we observed that all four PDC bit nozzles were plugged and half of the XCB shoe nozzles were plugged. It is possible that these were plugged during the test while coring Hole 942A, and the test results are anomalous. We assume that the low circulating rate would have prevented any effective valve operation.

Hole 942B

We offset the ship about 10 m to the east, positioned the bit at 3355.0 mbrf, and spudded Hole 942B at 1325 hr 10 May. Core 1H

recovered 7.45 m, and the mud line was defined to be at 3357.1 m. Cores 1H through 8H were taken from 3357.1 to 3431.0 mbrf (0–74.0 mbsf) and recovered 56.91 m (76.9% recovery). Only Cores 7H and 8H were oriented with the Tensor tool. Cores 5H and 6H recovered no core, although this interval was recovered in both Holes 942A and 942C, suggesting a mechanical problem.

Hole 942C

We offset the ship about 20 m to the west, positioned the bit at 3355.0 mbrf, and spudded Hole 942C at 2000 hr 10 May. Hole 942C was designed to get additional mud-line cores, to recover sediment from an interval that was incompletely recovered in Holes 942A and 942B, and to obtain additional material from a deep hemipelagic interval. Core 1H was 4.30 m, and the mud line was defined to be at 3360.2 mbrf. Based on lithologic and magnetic correlation, it is apparent that the following “reported” depths for Cores 2H through 5H and for the seafloor depth below sea level are approximately 4 m too shallow. This may have been caused by cored sediment falling out of the mud-line core (Core 942C-1H) during retrieval or an undetected partial stroke of the core barrel. Cores 1H and 2H were taken from 3360.2 to 3374.0 mbrf (0–13.8 mbsf). The hole was drilled (without coring) from 3374.0 to 3396.2 mbrf (13.8–36.0 mbsf). Cores 3H and 4H were taken from 3396.2 to 3415.2 mbrf (36.0–55.0 mbsf). The hole was drilled from 3415.2 to 3422.2 mbrf (55.0–62.0 mbsf), and Core 5H was taken from 3422.2 to 3431.7 mbrf (62.0–71.5 mbsf). In

Table 1. Site 942 coring summary.

Core	Date (1994)	Time (UTC)	Depth (mbsf)	Length cored (m)	Length recovered (m)	Recovery (%)
155-942A-						
1H	May 9	1920	0.0–3.8	3.8	3.78	99.5
2H	May 9	2000	3.8–13.3	9.5	9.02	94.9
3H	May 9	2050	13.3–22.8	9.5	9.83	103.0
4H	May 9	2140	22.8–32.3	9.5	9.96	105.0
5H	May 9	2225	32.3–41.8	9.5	9.67	102.0
6H	May 9	2340	41.8–51.3	9.5	9.62	101.0
7H	May 10	0030	51.3–60.8	9.5	9.84	103.0
8H	May 10	0115	60.8–70.3	9.5	9.59	101.0
9H	May 10	0250	70.3–79.8	9.5	9.61	101.0
10H	May 10	0350	79.8–89.3	9.5	10.30	108.4
11H	May 10	0440	89.3–98.8	9.5	8.27	87.0
12H	May 10	0540	98.8–104.0	5.2	5.47	105.0
13X	May 10	0720	104.0–110.1	6.1	5.00	81.9
14X	May 10	0820	110.1–119.7	9.6	4.71	49.0
15X	May 10	0930	119.7–129.3	9.6	6.50	67.7
16X	May 10	1025	129.3–139.0	9.7	6.50	67.0
17X	May 10	1135	139.0–148.6	9.6	6.50	67.7
18X	May 10	1255	148.6–158.3	9.7	7.54	77.7
19X	May 10	1410	158.3–167.9	9.6	7.51	78.2
20X	May 10	1525	167.9–177.6	9.7	3.38	34.9
Coring totals				177.6	152.6	85.9
155-942B-						
1H	May 10	1740	0.0–7.5	7.5	7.45	99.3
2H	May 10	1815	7.5–17.0	9.5	9.44	99.3
3H	May 10	1905	17.0–26.5	9.5	9.10	95.8
4H	May 10	1945	26.5–36.0	9.5	9.75	102.0
5H	May 10	2025	36.0–45.5	9.5	0.00	0.0
6H	May 10	2110	45.5–55.0	9.5	1.21	12.7
7H	May 10	2200	55.0–64.5	9.5	9.78	103.0
8H	May 10	2250	64.5–74.0	9.5	10.18	107.1
Coring totals				74.0	56.9	76.90
155-942C-						
1H	May 11	0200	0.0–4.3	4.3	4.30	100.0
2H	May 11	0055	4.3–13.8	9.5	9.72	102.0
3H	May 11	0210	36.0–45.5	9.5	9.74	102.0
4H	May 11	0255	45.5–55.0	9.5	10.00	105.2
5H	May 11	0355	62.0–71.5	9.5	10.27	108.1
Coring totals				42.3	44.0	104.10

Note: An expanded version of this coring summary table that includes lengths and depths of sections, location of whole-round samples, and comments on sampling disturbance is included on the CD-ROM in the back pocket of this volume.

all, we drilled 29.2 m, cored 42.3 m, and recovered 44.03 m (104.1%). Cores 3H through 5H were oriented using the Tensor tool. There was one imploded liner top. The bit cleared the rig floor at 0730 hr 11 May.

LITHOSTRATIGRAPHY

Introduction

Holes 942A, 942B, and 942C penetrate upper Quaternary sediment of a channel-levee system at the western edge of the middle Amazon Fan. It is uncertain whether this channel-levee system belongs to any of the channel-levee complexes on the Amazon Fan. In Hole 942A, sediment was recovered to a depth of 171.28 mbsf; a few intervals of nonrecovery occur below 100 mbsf, where XCB coring was done (Fig. 5). Hole 942B was intended to provide overlapping sediment cores in the upper 70 m of Hole 942A, but failed to recover any sediment in Cores 942B-5H and -6H. Hole 942C recovered sediment equivalent to the first two cores of Hole 942A and was then alternately drilled and cored in an attempt to retrieve sediment from the intervals that were not recovered completely in Hole 942B and to obtain a third sample of a carbonate layer at about 65 mbsf (see "Operations" section, this chapter).

The targeted carbonate-rich interval that was predicted to be at about 65 mbsf in Hole 942C was only partly recovered. Correlation of lithologic boundaries and magnetic susceptibility data (Fig. 20)

show an unexpected offset of about 4 m between correlative levels in Holes 942A and 942B compared with Hole 942C (there is at most only 1 m apparent offset between features in Holes 942A and 942B). The offset occurs below Core 942C-1H; in Core 942C-2H and deeper, all correlative features occur about 4 m shallower in Hole 942C than in either of the other two holes. In Hole 942C, either there was an abbreviated stratigraphic section near the top of the hole, or Core 942C-1H was incompletely recovered. The latter explanation is preferred because the reported water depth at Hole 942C is 3 m deeper than that at the other two holes, even though the distance between holes is small and 3.5-kHz profiles indicate a relatively flat seafloor at the site.

The six lithostratigraphic units defined at Site 942 are somewhat different from those at other Leg 155 sites because of the slower sedimentation rate at this site and the occurrence of several intervals rich in biogenic carbonate. These carbonate-rich intervals, although thin, either are recognized as separate units or are used to define the tops of units. This division emphasizes the potential paleoclimatic significance of the biogenic carbonate deposits. Two units (I and V) are calcareous clays. Unit II is apparently time-equivalent to the Upper Levee Complex of the Amazon Fan (see "Leg Synthesis" chapter, this volume). Units III and IV are turbidite sequences with carbonate-rich tops. Unit VI is essentially a fine-grained siliciclastic unit, distinct in its facies from all the other units and similar to distal levee deposits of the Amazon Fan.

The following lithostratigraphic descriptions, sub-bottom depths, and summary diagrams (Figs. 5 and 6) are based mainly on Hole 942A. Data from other holes are referred to only where essential for the complete description of lithologic characteristics.

Description of Lithostratigraphic Units

Unit I

Intervals: 155-942A-1H-1, 0–66 cm; 155-942B-1H-1, 0–81 cm; 155-942C-1H-1, 0–74 cm
Age: Holocene
Depth: 0.00–0.66 mbsf

Unit I consists of a brown (10YR 5/3) foraminifer-nannofossil clay (0.00–0.41 mbsf) that grades into an olive gray (5Y 5/2) nannofossil-rich clay (0.41–0.63 mbsf) with intense burrowing. Both overlie a faintly laminated, 3-cm-thick interval (0.63–0.66 mbsf) that is stained brown (10YR 4/3) by diagenetic iron oxyhydroxides. At Holes 942B (0.77–0.81 mbsf) and 942C (0.72–0.74 mbsf), there is a well-developed, brown (10YR 4/3), diagenetic iron-rich crust at the base of Unit I, similar to the crust that was recovered at most other Leg 155 sites from a similar sub-bottom depth. This iron-rich crust was analyzed previously and correlated throughout the Amazon Fan and adjacent Guiana Basin (e.g., Damuth, 1977; see "Introduction" chapter, this volume).

Unit II

Intervals: 155-942A-1H-1, 66 cm, through -4H-4, 80 cm; 155-942B-1H-1, 81 cm, through -4H-1, 103 cm; 155-942C-1H-1, 74 cm, through -2H-CC
Age: ?Holocene to late Pleistocene
Depth: 0.66–28.10 mbsf

Unit II consists predominantly of terrigenous clay, silty clay, silt, and very fine sand (Figs. 5 and 6). The carbonate content of Unit II is generally 1.4% to 4.5% (see "Organic Geochemistry" section, this chapter). Sediment color ranges from dark gray (5Y 4/1) to very dark gray (5Y 3/1). Burrows, mottles (on a centimeter scale), and friable soft micromodules a few millimeters in diameter occur in varying abundance throughout much of Unit II and generally are black (either N 2/0 where color boundaries are sharp, or 5Y 2.5/1 where less dis-

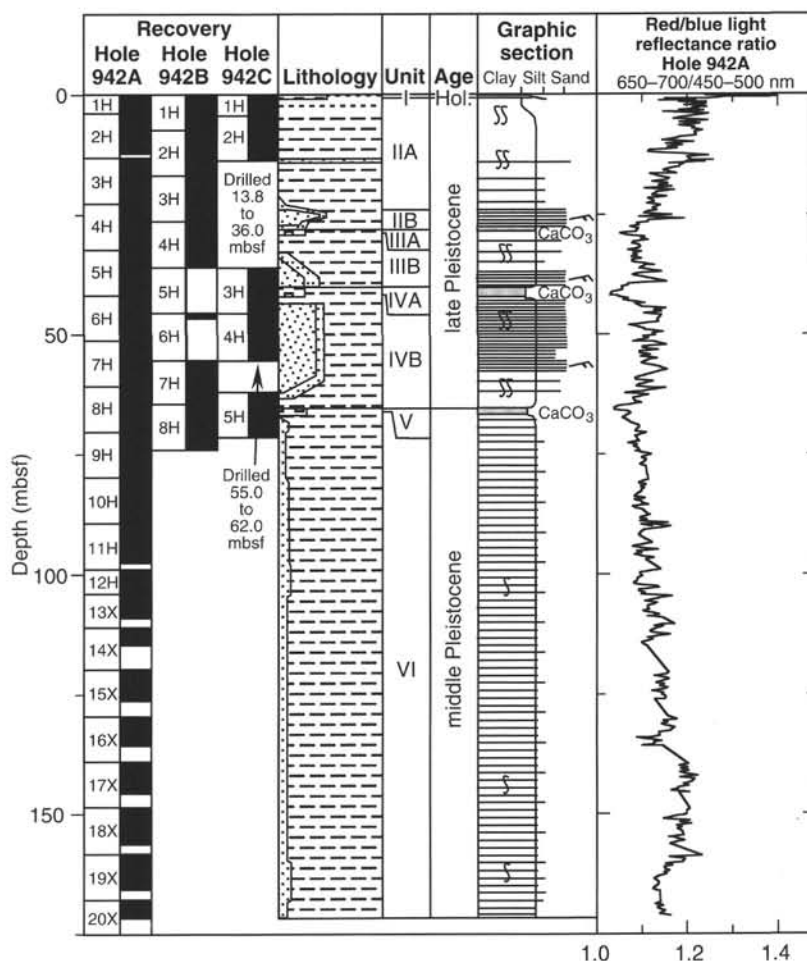


Figure 5. Composite stratigraphic section for Site 942 showing core recovery, a simplified summary of lithology primarily for Hole 942A, depths of unit boundaries, age, a graphic section with generalized grain-size and bedding characteristics, and downhole variations in light-reflectance values. The lithologic symbols are explained in Figure 1 of the “Explanatory Notes” chapter (this volume).

tinct). Most black stains are caused by diagenetic hydrotroilite, which imparts an ephemeral black color (N 2/0) to the sediment (see “Introduction” chapter, this volume).

Unit II is divided into two subunits based on the occurrence of the shallowest sand bed (Figs. 5 and 6). This sand bed was used to define the top of Subunit IIB because large burrows (*Echinocardium*) appear to have destroyed parts of thinner layers so that they cannot be correlated between Holes 942A and 942B. For example, the silt bed that is about 7 m above the shallowest sand bed in Hole 942A could not be identified in Hole 942B. In contrast, the sand bed at the top of Unit II, and several beds below this bed, are present with similar thicknesses in both holes.

Subunit IIA

Subunit IIA extends from the base of Unit I at 0.66 mbsf to a depth of 23.85 mbsf (interval 942A-1H-1, 66 cm, through 942A-4H-1, 105 cm). This subunit consists of dark gray clay (5Y 4/1) with distinct black (N 2/0) mottles and burrows (e.g., Section 942A-1H-2), grading to silty clay by 4 mbsf.

An anomalous, 50-cm-thick, structureless and soupy, very fine sand bed in Hole 942A (bed base at 14.05 mbsf; interval 942A-3H-1, 31–80 cm) is only 11 cm thick in Hole 942B (bed base at 14.70 mbsf; interval 942B-2H-5, 109–120 cm) and 7 cm thick in Hole 942C (bed base at 9.57 mbsf; interval 942C-2H-4, 70–77 cm). This bed is well above the first occurrence of silt beds in any hole (e.g., Fig. 6) and therefore was not used to define the top of Subunit IIB. The greater thickness of this bed in Hole 942A is probably a result of flow-in during coring. Evidence for sand redistribution in Core 942A-3H in-

cludes a sand-filled crack 10 cm below the base of the sand bed and a smear of sand grains along the core liner to a depth about 2 m below the base of the sand bed.

The shallowest silt bed occurs at 17.64 mbsf (interval 942A-3H-3, 134–135 cm). The frequency of silt and sand layers in Subunit IIA is two per meter just below Section 942A-3H to four per meter near the base of the subunit. Some of the silt beds contain cross-lamination.

Subunit IIB

Subunit IIB extends from 23.85 to 28.10 mbsf (interval 942A-4H-1, 105 cm, through 942A-4H-4, 80 cm) and is characterized by dark gray (5Y 4/1) to very dark gray (5Y 3/1) silty clay interbedded with sharp-based graded beds with very fine sand bases and silt tops (Fig. 7). There are also some silt beds and laminae. Sand beds, 1 to 13 cm thick, locally form about 50% of core sections (e.g., Section 942-4H-2). Some beds have basal flute casts and many are cross-laminated (Fig. 8).

Unit III

Intervals: 155-942A-4H-4, 80 cm, through -5H-7, 10 cm; 155-942B-4H-1, 103 cm, through -4H-CC
 Age: late Pleistocene
 Depth: 28.10–40.18 mbsf

Unit III consists of a thin carbonate-rich interval underlain by a siliciclastic interval of silty clay containing silt laminae and beds of very fine sand and silt. Unit III is divided into two subunits.

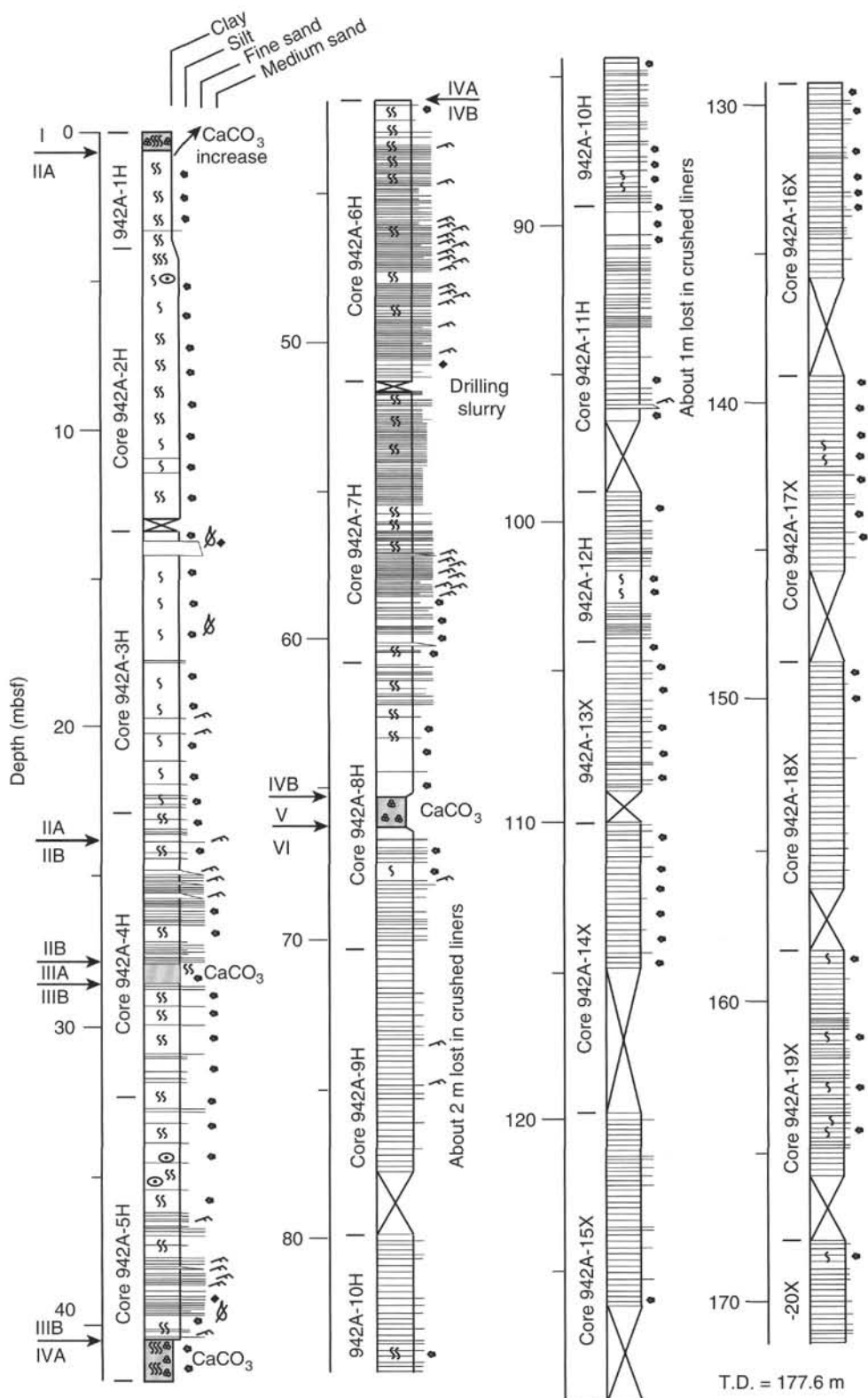


Figure 6. Graphic sedimentological columns for Site 942 showing grain-size variation (width of columns), bed thickness, and sedimentary structures; symbols and preparation of these columns are explained in the "Lithostratigraphy" section of the "Explanatory Notes" chapter, this volume). Arrows indicate the positions of unit and subunit boundaries.

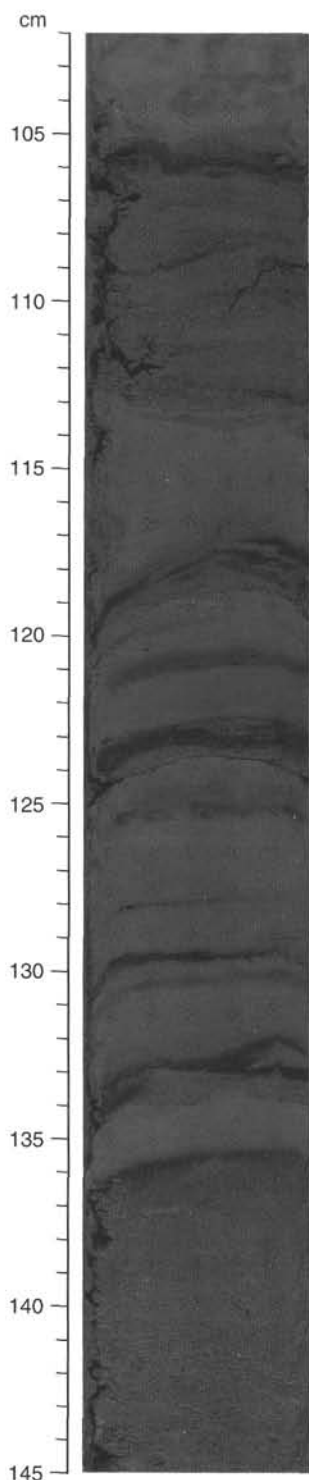


Figure 7. Normally graded beds of very fine sand through silt in Subunit IIB (942A-4H-2, 102–145 cm). The cross-lamination at 108–110 cm is interpreted as resulting from scour and fill processes and, therefore, cannot be used to determine paleoflow direction.

Subunit IIIA

Subunit IIIA extends from 28.10 to 28.80 mbsf (interval 942A-4H-4, 80–150 cm) and consists of gray (5Y 5/1) foraminifer-nannofossil-rich silty clay. This subunit was also recovered in Hole 942B (interval 942B-4H-1, 103 cm, to -2, 20 cm). The carbonate content is 14.2% in Sample 942B-4H-1, 148–150 cm. Subunit IIIA passes transitionally downward into Subunit IIIB. The sediment color becomes darker across the transition, and the abundance of biogenic components decreases to background levels for siliciclastic sediment at the site.

Subunit IIIB

Subunit IIIB (28.80–40.18 mbsf, interval 942A-4H-4, 150 cm, through -5H-7, 10 cm) consists of bioturbated dark gray silty clay (5Y 4/1), mottled by hydrotroilite, interbedded with silt laminae and beds of silt and very fine sand. Sample 942A-5H-1, 47–49 cm, contains 1.7% carbonate. *Spreiten* burrows (?*Echinocardium*) commonly disrupt the tops of the very fine sand beds, except in the most sandy intervals. Sand and silt beds are less than 8 cm thick. In about 60% of the subunit, the sand and silt beds average two per meter; however, toward the base (in particular Sections 942A-5H-4 through -5H-6), sand and silt beds increase in frequency to an average of five per meter and constitute as much as 40% of short intervals. Many of the sand beds are cross-laminated (Fig. 9).

Unit IV

Intervals: 155-942A-5H-7, 10 cm, through -8H-3, 140 cm; 155-942B-6H-1, 0 cm, through -8H-1, 22 cm; 155-942C-3H-1, 0 cm, through -4H
Age: late Pleistocene
Depth: 40.18–65.20 mbsf

Unit IV consists of a thin carbonate-rich interval underlain by a siliciclastic interval of silty clay with beds and laminae of very fine sand and silt. In contrast to Unit III, the sand and silt beds compose most of the unit, with muddier intervals restricted mainly to the base and top of the unit. Unit IV is divided into two subunits based mainly on carbonate content and color of the sediment.

Subunit IVA

Subunit IVA extends from 40.18 to 41.80 mbsf (interval 942A-5H-7, 10 cm, through -6H-1, 0 cm). The sediment is characterized by dark gray (5Y 4/1) to dark greenish-gray (5GY 4/1) foraminifer-nannofossil-bearing clay and foraminifer-nannofossil-rich clay. A carbonate content of 8.7% was determined for the upper dark gray part of Subunit IVA (Sample 942A-5H-7, 46–47 cm); the lower, more carbonate-rich part (below Section 942A-5H-7 at 90 cm) is estimated to contain about 15% carbonate, based on examination of a smear slide from this interval. All but the top of Subunit IVA was recovered in Hole 942C (interval 942C-3H-1, 0 cm, through -3H-2, 103 cm); this subunit was not recovered in Hole 942B. Subunit IVA passes transitionally to Subunit IVB, both in color and in visible biogenic components. In Hole 942C, the color changes downward from dark gray (2.5Y 4/1) to dark olive gray (5Y 3/2). Spectrophotometer color data (Fig. 5) record this color change.

Subunit IVB

Subunit IVB extends from 41.80 to 65.20 mbsf (interval 942A-6H-1, 0 cm, through -8H-3, 140 cm). The sediment consists of intensely burrowed, dark greenish gray silty clay (5GY 4/1), which alternates with beds and laminae of very fine sand and coarse silt. The carbonate content is 0.8% to 2.0%. *Spreiten* burrows, up to 3 cm thick and crossing the entire core diameter, generally occur along the tops of silt or sand beds, locally destroying these beds (Figs. 10 and 11). At the top of Subunit IVB, there are generally two silt or sand beds

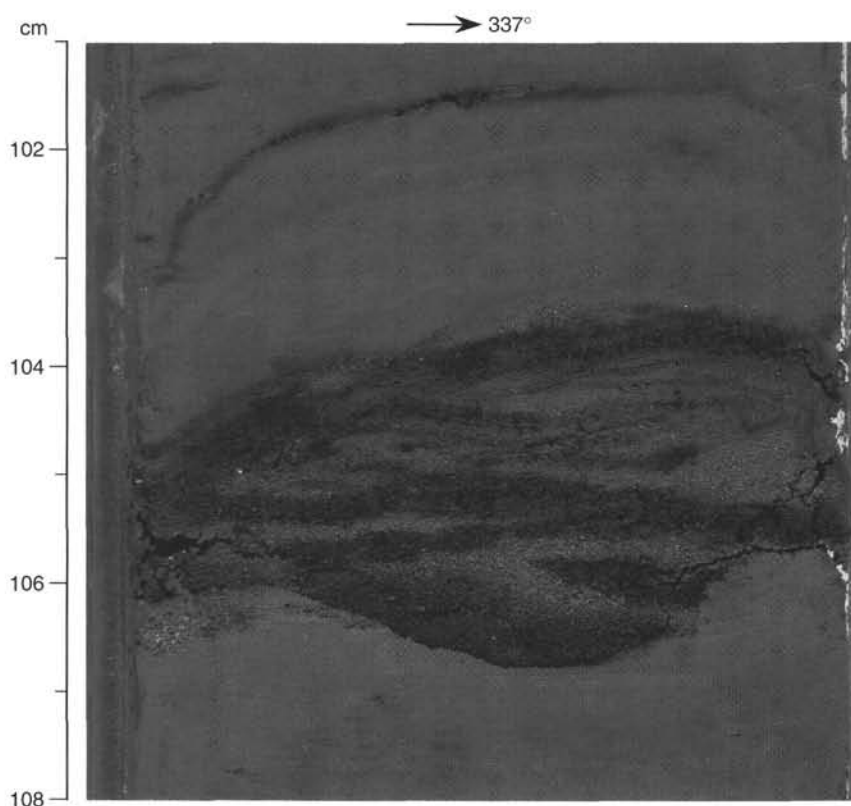


Figure 8. Cross-laminated bed of very fine sand in Subunit IIB (942A-4H-1, 101–108 cm). The basal scour may be a transverse cross section of a flute cast. The apparent migration direction of ripples in this oriented APC core is toward 337°.

per meter. At 43.30 mbsf (Section 942A-6H-2 at 0 cm), the density of beds increases abruptly to 16 per meter and averages about 15 beds per meter to the base of Section 942A-7H-5 at 58.80 mbsf. Below this depth, beds of very fine sand and silt are still abundant (about five per meter) but decrease sharply from 62.30 mbsf (Section 942A-8H-1) to the base of the subunit. Most sand and silt beds are cross-laminated (Figs. 11 and 12).

Unit V

Intervals: 155-942A-8H-3, 140 cm, through -4, 77 cm; 155-942B-8H-1, 22–126 cm; 155-942C-5H-1, 0–125 cm
Age: late Pleistocene
Depth: 65.20–66.07 mbsf

Unit V consists of foraminifer-nannofossil clay and foraminifer-nannofossil-rich clay (12.5%, 26.2%, and 31.7% carbonate, respectively, in Samples 942B-8H-1, 120–125 cm, 942B-8H-1, 80–90 cm, and 942C-5H-1, 0–10 cm). The greenish-gray color of the sediment (5GY 6/1 to 5GY 5/1) contrasts with the darker greenish gray silty clay of the units above and below. In interval 942A-8H-4, 41–77 cm, where carbonate content is highest, abundant foraminifer tests are visible on the core surface.

Unit VI

Intervals: 155-942A-8H-4, 77 cm, through -20X-CC (bottom of hole); 155-942B-8H-1, 126 cm, through -8H-CC (bottom of hole); 155-942C-5H-1, 125 cm, through -5H-CC (bottom of hole)
Age: middle Pleistocene
Depth: 66.07–171.28 mbsf

Unit VI is a homogeneous, dark gray (5Y 4/1), color-banded and laminated silty clay with silt laminae and only a few thin silt beds (maximum 3 cm thick). Dark color bands in the laminated silty clays are 1 to 2 cm apart and about 0.5 cm thick and are accentuated by dis-

seminated black (N 2/0) hydrotroilite. Color mottling is common. The carbonate content is generally low; the range of 16 samples is 0.7% to 3.9%, except for two anomalously high values of 14.2% and 16.4% from lighter colored tops of very thin turbidite beds. XRD analysis indicates that these relatively high carbonate contents are caused by diagenetic siderite.

Mineralogy

Silty clay forms a major part of Units II and VI and Subunits IIIB and IVB. The composition of the silt fraction in these silty clays, from smear slides, is 50%–65% quartz, 1%–15% feldspar, 0%–8% mica, and 7%–10% accessory minerals. Organic detritus, foraminifers, and sponge spicules compose less than 5% of any sample. The accessory minerals include common hornblende and enstatite and rare zircon and hypersthene.

Bulk XRD analysis was performed on 17 samples of silty clay from Cores 942A-1H through -20X (Table 2). The common minerals throughout the cored succession, based on the relative intensities of their primary peaks (normalized to quartz intensity), are quartz, plagioclase, augite, and the clay minerals smectite, illite (+ mica), and kaolinite. A few samples contain calcite and K-feldspar. Except for differences in the content of clay minerals, the major mineral groups show little variation with depth (Fig. 13A). The relative abundances of clay minerals are fairly constant below about 40 mbsf, in Units IV through VI (Fig. 13B). There appears to be irregular variation in Units II and III, particularly in smectite abundance. A diagenetic nodule from 48.24 mbsf in Subunit IVB has a strong diffraction peak at $13.3^\circ 2\theta$, characteristic of the phosphate mineral vivianite.

Spectrophotometry

Light-reflectance levels of the brown calcareous clay in Unit I reach 35%, whereas those of the dark olive gray to very dark gray sediment in Unit II range between 15% and 25%. The ratio between

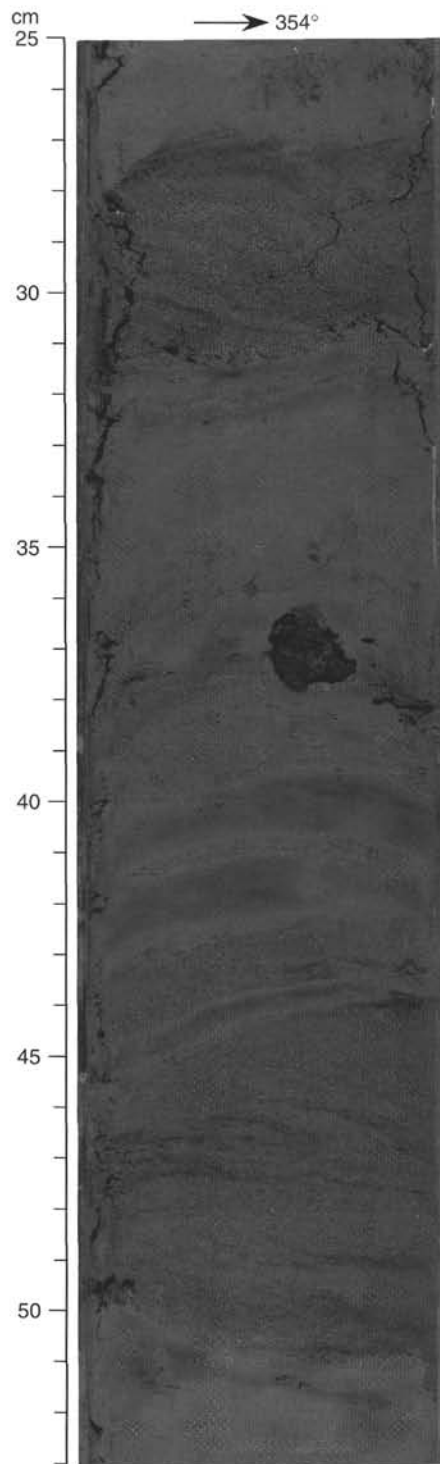


Figure 9. Cross-laminated sand beds in Subunit IIIB (942A-5H-5, 25–53 cm). Several beds have burrow-modified tops (e.g., at 25 cm), and others have been almost completely obliterated by burrowers (e.g., at 35–40 cm). The apparent migration direction of ripples in this oriented APC core is toward 354°. The black nodule at 36–38 cm is composed of hydrotroilite.

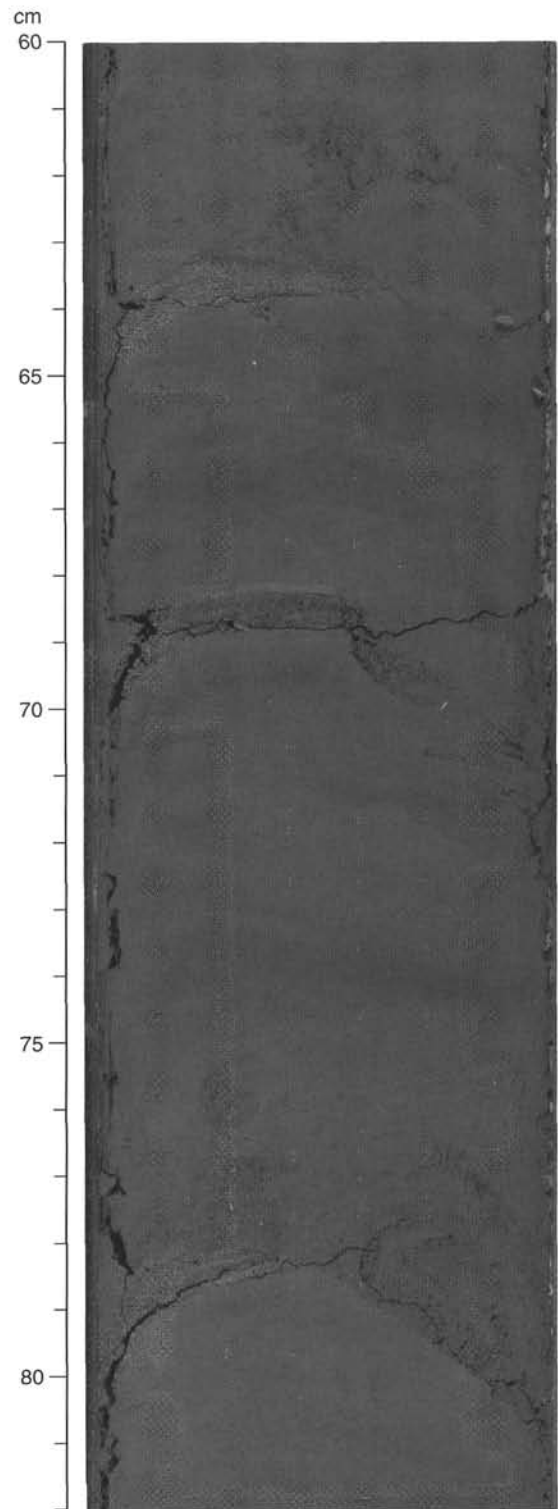


Figure 10. Burrow-truncated, very fine sand laminae in Subunit IVB (942A-7H-4, 60–82 cm). These *Spreiten* burrows are thought to have been produced by echinoids.

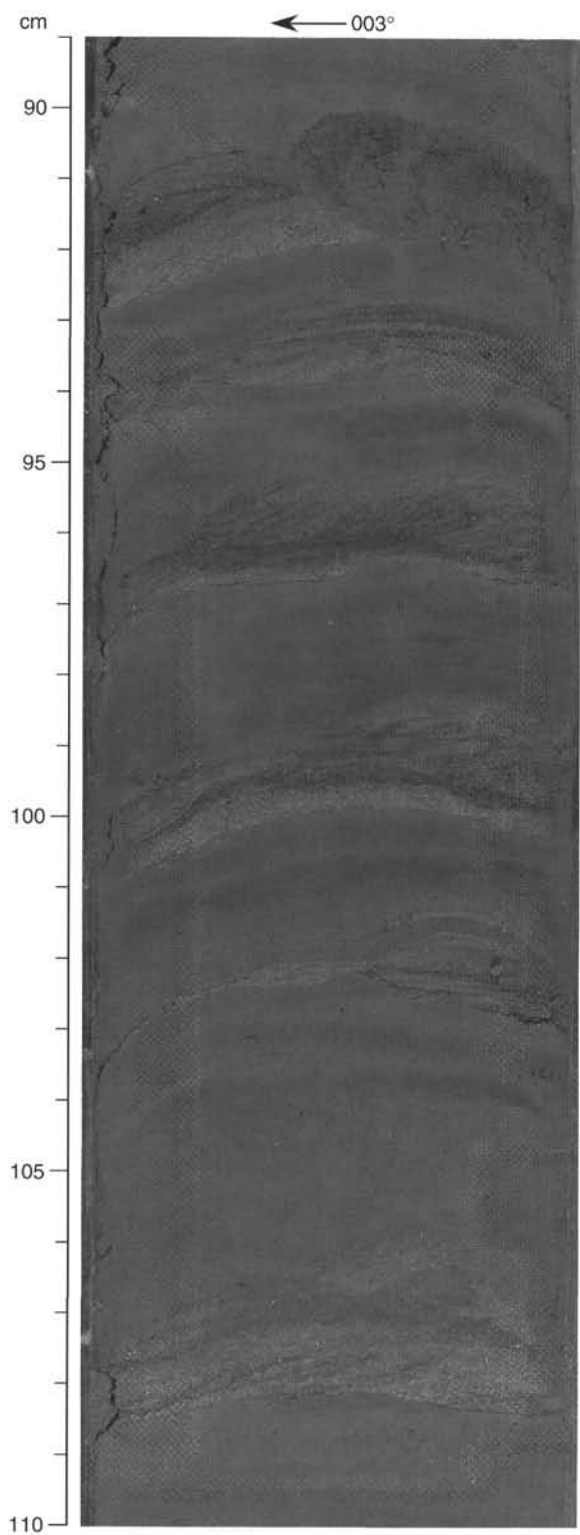


Figure 11. Cross-laminated, wavy laminae and beds of very fine sand in Sub-unit IVB (155-942A-6H-5, 89–110 cm). Note the finely laminated mud immediately above some beds (e.g., at 93 and 102 cm), “fading” ripple lamination at 99 cm, and burrow truncation of one bed at 90–92 cm. The apparent migration direction of ripples in this oriented APC core is toward 003°.

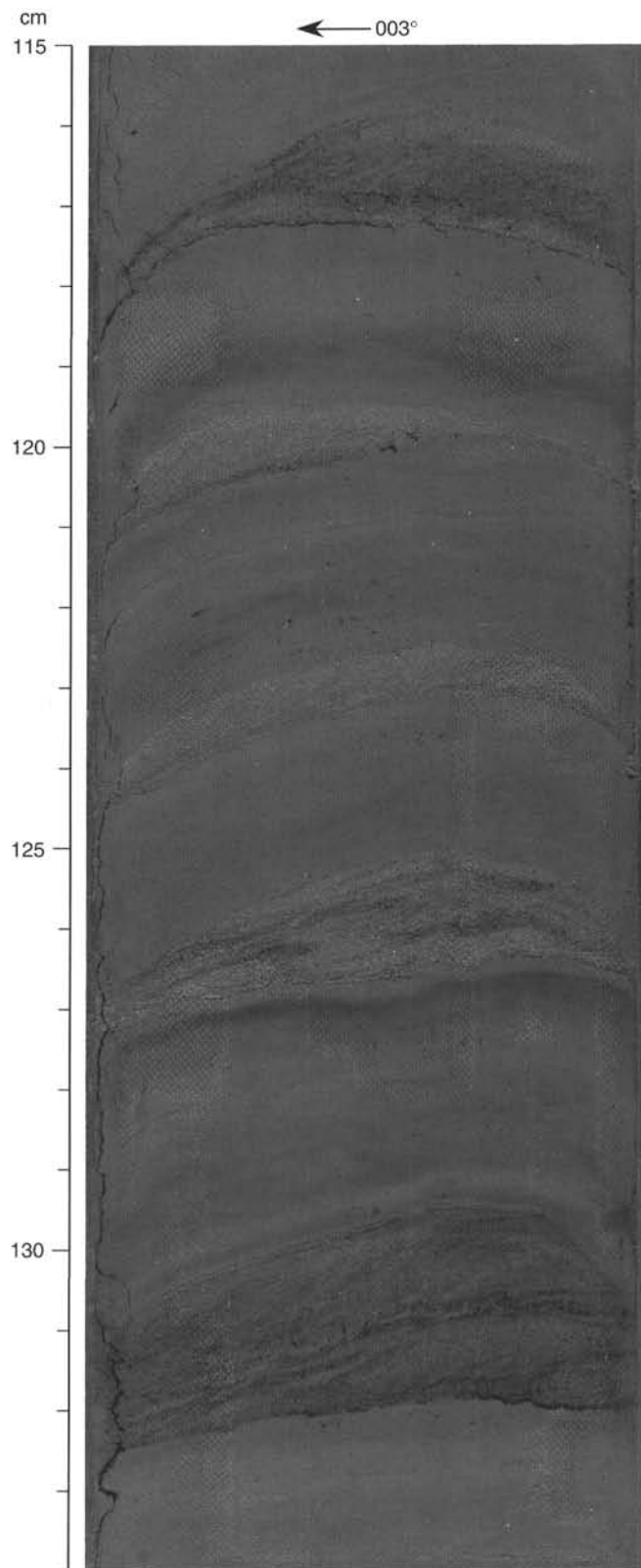


Figure 12. Cross-laminated, wavy laminae and beds of very fine sand in Sub-unit IVB (942A-6H-4, 115–134 cm). Note the finely laminated mud immediately above most of these rippled divisions, and the “fading” ripple lamination at 116 cm. The apparent migration direction of ripples in this oriented APC core is toward 003°.

Table 2. Relative peak intensities of main minerals within major lithologies at Site 942.

Core, section, interval (cm)	Depth (mbsf)	Relative intensity of primary peaks								
		Smectite	Mica + Illite	Kaolinite	Quartz	Plagioclase	K-feldspar	Augite	Hornblende	Calcite
155-942A-										
1H-3, 36-37	3.36	9.7	18.6	9.9	100.0	7.1	7.4	3.1	*	*
2H-4, 55-56	8.85	7.2	13.3	12.4	100.0	11.9	*	*	*	15.0
3H-4, 101-103	18.81	32.0	18.5	13.7	100.0	10.8	*	*	*	5.9
4H-3, 68-69	26.48	13.6	16.3	11.9	100.0	8.0	*	3.5	*	*
6H-3, 82-83	45.62	7.3	16.0	9.4	100.0	6.2	*	2.1	*	*
7H-5, 57-59	57.87	7.5	16.6	9.6	100.0	9.1	4.5	2.4	*	1.6
9H-5, 82-83	74.99	10.5	16.6	10.1	100.0	8.6	3.2	2.1	*	*
10H-2, 96-97	82.26	15.3	21.3	11.4	100.0	9.8	*	3.6	*	*
11H-4, 81-82	93.58	9.3	19.4	12.4	100.0	11.1	*	2.9	*	*
13X-2, 50-51	106.00	9.2	25.5	16.5	100.0	10.1	*	3.5	*	*
14X-1, 78-79	110.88	10.0	21.1	14.0	100.0	10.2	*	3.2	*	*
15X-3, 60-61	123.30	17.2	21.0	16.9	100.0	10.0	*	3.2	*	*
16X-3, 79-80	133.09	12.9	15.3	15.5	100.0	10.5	*	4.0	*	7.7
17X-3, 78-79	142.78	11.7	21.8	13.6	100.0	9.0	*	3.0	*	*
18X-3, 18-19	151.78	13.6	20.4	13.4	100.0	9.3	*	3.5	*	*
19X-1, 90-91	159.20	11.1	27.3	15.6	100.0	9.4	5.6	3.1	5.5	*
20X-1, 78-79	168.68	20.3	44.8	21.9	100.0	10.1	*	3.6	*	*

Notes: See "Lithostratigraphy" section in the "Explanatory Notes" chapter, this volume, for XRD methods. * = non-detection.

red (650–700 nm) and blue (450–500 nm) spectral reflectance averages 1.14 (Fig. 5). The highest red/blue ratio is measured in the brownish gray calcareous clay of Unit I. Enhanced red reflectance also coincides with thick silt and sand beds of Units II, III, and IV, and originates from iron oxide stained quartz grains. The lowest values of the red/blue ratio correspond to the carbonate-rich sediment of Subunits IIIA and IVA and Unit V, which are greenish gray to dark greenish gray (5GY 6/1 to 5GY 4/1) because of the presence of reduced-iron phases. The stratigraphic limits of these low red/blue ratios associated with the carbonate-rich clays of Subunit IVA and Unit V extend across both the unit boundaries. For example, Subunit IVA extends from 40.18 to 41.80 mbsf, whereas the red/blue ratio is lower

than average from 39.50 to 42.80 mbsf. Except for the carbonate-rich units, other correlations between lithologic units and the red/blue ratio do not exist or are masked by the high-frequency variability of the reflectance record (see Schneider et al., this volume).

Discussion

The carbonate-rich sediment of Units I and V and Subunits IIIA and IVA represents intervals of relatively slow sediment accumulation (i.e., "condensed sections") that were deposited during times of reduced siliciclastic influx. Unit V, in particular, with high carbonate content similar to Holocene levels, was probably deposited during a sea-level highstand. The color-banded and laminated silty clays of Unit VI are lithologically similar to the upper parts of levees at other Leg 155 sites and suggest deposition from frequent overbank-flow of turbidity currents during levee construction. Deposits of Units I through V rest on the underlying morphology of the Unit VI levee.

The sand turbidites of Unit II and Subunits IIIB and IVB are characterized by ripple lamination and have undergone moderately intense burrowing (?*Echinocardium*). Ripple migration direction in oriented cores is toward the north-northwest, based on four determinations of apparent foreset dip: 337°, 354°, two toward 003° (Figs. 8, 9, 11, 12). This direction is down the regional slope, but toward the axis of the buried channel that is associated with Unit VI (Fig. 4). Burrowed sand-rich sediment with abundant current ripples is generally uncommon at other Leg 155 sites. The burrow intensity may reflect the relatively slow sedimentation rates at this site compared to those at other Leg 155 sites (see "Biostratigraphy" section, this chapter). The current ripples are at the tops of sharp-based, normally graded sand beds that, unless burrowed at their tops, pass abruptly upward into silt-mud laminae of Bouma (1962) division d (Figs. 11 and 12). Hence, these ripples were apparently produced by the overflow of channelized turbidity currents, not by slow reworking of the tops of turbidites by bottom currents. The ripple lamination probably is more abundant here than at other sites because the dominant grain size is fine sand, rather than silt. Experimental flume studies indicate that current ripples are stable over a wide range of flow velocity in fine sand, but not in silt (Allen, 1984, p. 282).

The abundant sand turbidites in Subunits IIB, IIIB, and IVB have not been encountered at other Leg 155 sites and may indicate a different source of sediment supply at this site. These turbidites commonly occur immediately above carbonate-rich units, at least one of which (Unit V) is interpreted as a high-stand deposit. The sand fraction in the turbidites at this site may have been derived by erosion of a transgressive sand sheet that remained on the shelf after the sea-level rise that culminated with the deposition of the carbonate-rich Unit

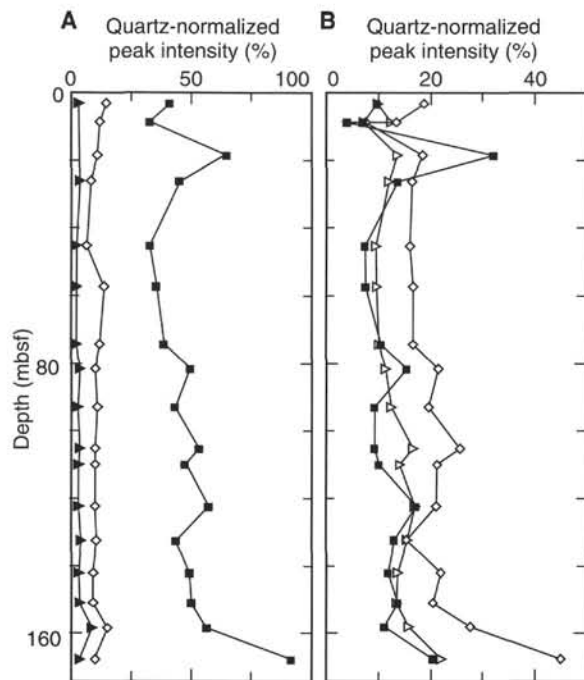


Figure 13. Variations in XRD mineralogy in Hole 942A. A. Downhole variation in the relative peak intensities of the main mineral groups, based on data in Table 2. Squares = clay minerals + mica; diamonds = feldspar; triangles = augite + hornblende. B. Downhole variation in the relative peak intensities of clay minerals and micas. Squares = smectite; diamonds = mica + illite; triangles = kaolinite.

Table 3. Calcareous nannofossil and siliceous microfossil abundance data for Holes 942A, 942B, and 942C.

Core, section, interval (cm)	Top interval (mbsf)	Bottom interval (mbsf)	Calcareous nannofossils			Diatoms		Sponge spicules	Radiolarians	Ericson Zone (inferred from foraminifers)	Age (inferred from foraminifers)
			Abundance	Preservation	Zone	Marine	Fresh water				
155-942A-											
1H-MI, 0-0	0.00	0.00	a	g	CN15b	r	b	r	b	Z	Holocene
1H-1, 0-1	0.00	0.01	a	g		r	b	r	b	Z	Holocene
1H-1, 5-6	0.05	0.06	a	g		r	b	r	b	Z	Holocene
1H-1, 28-29	0.28	0.29	a	g		r	b	b	b	Z	Holocene
1H-1, 45-46	0.45	0.46	a	g		b	b	b	b	Z	Holocene
1H-1, 60-61	0.60	0.61	a	g		b	b	b	b	Z	Holocene
1H-1, 68-70	0.68	0.70	c	g		b	b	b	b	Z	Holocene
1H-1, 110-115	1.10	1.15	f	g		b	b	b	b	Z	Holocene
1H-2, 50-55	2.00	2.05	r	m		b	b	b	b	Z	Holocene
1H-2, 145-150	2.95	3.00	vr	p		b	b	b	b	Z	Holocene
1H-3, 50-52	3.50	3.52	vr	p		b	b	b	b	Z	Holocene
1H-CC, 12-19	3.68	3.77	r	m		b	b	b	b	Y	late Pleist.
2H-CC, 47-56	12.72	12.81	c	g		b	b	b	b	Y	late Pleist.
3H-CC, 18-27	22.94	23.03	r	m		b	b	b	b	Y	late Pleist.
4H-CC, 15-24	32.77	32.86	r	m		b	b	b	b	Y	late Pleist.
155-942A-											
5H-7, 137-142	41.46	41.51	a	g	CN15a	b	b	b	b	Y	late Pleist.
5H-CC, 35-44	41.87	41.96	a	g		b	b	b	b	X	late Pleist.
6H-CC, 35-44	51.32	51.41	r	m		b	b	b	b	X	late Pleist.
7H-CC, 3-12	61.04	61.13	tr	—		b	b	b	b	X	late Pleist.
8H-4, 9-10	65.39	65.40	f	g		b	b	b	b	X	late Pleist.
8H-4, 44-45	65.74	65.75	a	g		b	b	b	b	X	late Pleist.
8H-4, 62-62	65.92	65.92	a	g		b	b	b	b	X	late Pleist.
8X-CC, 18-27	70.29	70.38	tr	—		b	b	b	b	W	middle Pleist.
9H-4, 55-55	73.22	73.22	b	—		b	b	b	b	W	middle Pleist.
9H-5, 80-80	74.97	74.97	r	p		b	b	b	b	W	middle Pleist.
9H-CC, 32-41	77.49	77.58	b	—		b	b	b	b	W	middle Pleist.
10H-2, 124-124	82.54	82.54	b	—		b	b	b	b	W	middle Pleist.
10H-CC, 32-41	90.00	90.09	b	—		b	b	b	b	W	middle Pleist.
11H-CC, 19-28	96.86	96.85	b	—		b	b	b	b	W	middle Pleist.
12H-CC, 21-30	104.06	104.15	b	—		b	b	b	b	W	middle Pleist.
13X-CC, 10-19	108.90	108.99	b	—		b	b	b	b	W	middle Pleist.
14X-CC, 11-20	114.71	114.80	b	—		b	b	b	b	W	middle Pleist.
15X-CC, 12-21	126.10	126.19	b	—		b	b	b	b	W	middle Pleist.
16X-CC, 11-20	135.70	135.79	b	—		b	b	b	b	W	middle Pleist.
17X-CC, 11-21	145.40	145.49	tr	—		b	b	b	b	W	middle Pleist.
18X-CC, 9-18	156.04	156.13	vr	—	CN146b?	b	b	b	b	W	middle Pleist.
19X-CC, 10-19	165.71	165.80	b	—		b	b	b	b	W	middle Pleist.
20X-2				tr		b	b	b	b	W	middle Pleist.
20X-CC, 28-37	171.18	171.27	b	—		b	b	b	b	W	middle Pleist.
155-942B-											
1H-CC, 12-21	7.23	7.45	tr	—	CN15b					Y	late Pleist.
2H-CC, 9-18	16.76	16.95	vr	—						Y	late Pleist.
3H-CC, 0-9	26.00	26.10	tr	—						Y	late Pleist.
4H-CC, 11-20	36.08	36.29	c	g	CN15a					X	late Pleist.
6H-CC, 0-0	46.55	46.71	vr	—						X	late Pleist.
7H-CC, 2-11	64.50	64.78	vr	—						X	late Pleist.
8X-CC, 25-34	74.33	74.68	vr	—						W	middle Pleist.
155-942C-											
1H-MI			a	g	CN15b					Z	Holocene
1H-CC, 3-12	4.17	4.30	a	g						Y	late Pleist.
2H-CC, 11-20	13.81	14.02	c	g						X	middle Pleist.
3H-CC, 27-36	45.66	45.74	b	—						X	middle Pleist.
4H-CC, 12-21	55.13	55.50	b	—						X	middle Pleist.

V. Similar outer-shelf sand is present on the modern shelf, having formed during the Holocene sea-level rise (Milliman et al., 1975; Nittrouer et al., 1986). Subsequent lowering of sea level after deposition of Unit V could then have remobilized this sand into a shelf-edge canyon upslope from Site 942.

The greater abundance and cumulative thickness of sand turbidites in Subunit IVB, compared with those in Subunits IIB and IIIB, may reflect a progressively decreasing and sequential tapping of the coarse material that was stored along the outer shelf during the Unit V transgression. In this scenario, the basal, muddy part of Subunit IVB might correspond to the early phase of sea-level fall before the sand began to be supplied to the canyon head.

BIOSTRATIGRAPHY

Calcareous Nannofossils

An abundant, well-preserved, diverse nannofossil assemblage is present in the foraminifer-nannofossil clay of Unit I, and includes a high abundance of *Thoracosphaera* sp. (Table 3). A high abundance

of well-preserved nannofossils is found to a depth of 1.1 mbsf, well below the "iron-rich crust" (Sample 942A-1H-1, 110-112 cm). In the upper part of the glacial-age Unit II, nannofossils are rare (Samples 942A-1H-2, 50-55 cm [2.0 mbsf], through -2H-CC, 47-56 cm [3.7 mbsf]). Nannofossils reappear in high abundance in Unit II (Samples 942A-2H-2, 118-119 cm [4.5 mbsf], through -3H-2, 117-118 cm [23.9 mbsf]), suggesting a high pelagic component and thus differentiating this glacial-age sediment from others recovered during Leg 155. Samples through Subunits IIIA and IVA (Cores 942A-4H through -5H) reveal rapid changes in the abundance and preservation of calcareous nannofossils from barren intervals to those with a high abundance of well-preserved nannofossils. The nannofossil assemblage in Section 942A-4H-4 contains a nannoflora with a low abundance of *E. huxleyi*, which places Subunit IIIA as older than 85 ka. Samples taken from Subunit IVB (Cores 942A-6H and -7H) are almost barren of calcareous nannofossils. A carbonate-rich layer in Unit V (Section 942A-8H-4) contains a diversified and well-preserved nannoflora. This assemblage includes common but not dominant specimens of *Gephyrocapsa* sp. and is therefore slightly different from the *Gephyrocapsa*-dominated nannofossil assemblage

es seen in other "deep carbonate units" at Sites 931, 933, 935, and 936. The assemblages in this interval include common *G. oceanica* and relatively rare *E. huxleyi*, which constrains the age of this carbonate interval to a highstand period younger than 0.26 Ma (Zone CN15a). Closely spaced samples from Core 942A-8H show that the abundance and preservation of calcareous nannofossils vary significantly throughout Unit V.

Unit VI is characterized by a low abundance or absence of calcareous nannofossils (Samples 942A-8H-CC, 18–27 cm, through -20X-CC, 28–37 cm), which is indicative of glacial conditions. Sample 942A-18X-CC, 9–18 cm, is apparently lacking *E. huxleyi*, which will place the lower part of Unit IV in Zone CN14b. In Cores 942A-9H and -10H, layers of lighter colored clay are carbonate-rich intervals but contain rare or no calcareous nannofossils. XRD analyses show that these intervals are dominated by authigenic siderite. Where nannofossils are present in these intervals, one species (*C. leptoporus*) tends to show secondary overgrowth.

Planktonic Foraminifers

Unit I is a calcareous clay that contains abundant and well-preserved foraminifers (Table 4). The boundary between Ericson Zones Z and Y (disappearance of *G. tumida*) occurs between the mud line and 3.77 mbsf (between Sample 942A-1H-1, 0–1 cm, and -CC, 12–19 cm). *G. tumida* and *G. menardii* are absent in the lower part of Subunit IIA through Unit III from 3.77 to 32.8 mbsf (Samples 942A-1H-CC, 12–19 cm, through -4H-CC, 24 cm), and this interval has been defined as the Ericson Y Zone. Mica, fine wood fragments, pteropods, and black authigenic mineral nodules are found in this zone. *P. obliquiloculata* reappears in Subunit IIA (Sample 942A-3H-CC, 18–27 cm), and the 40-ka $Y_{p.obliq.}$ datum has been placed at 23 mbsf. In Units IV and V, *G. tumida* and *G. menardii* are present from 41.9 to 65.9 mbsf (Samples 942A-5H-CC, 35–44 cm, through -8H-4, 60–62 cm), defining this interval as an interglacial section (Ericson X Zone; 85–130 ka). Mica, fine wood fragments, and calcareous spines are present in Units IV and V. *G. tumida flexuosa* is indicative of peak interglacial conditions, especially the last interglacial. At 65.9 mbsf in Unit V (Sample 942A-8H-4, 60–62 cm) *G. tumida* and *G. menardii* are present, but *G. tumida flexuosa* is absent. This interval represents the transition period between the interglacial X Zone and the glacial W Zone. *G. tumida*, *G. menardii*, and *G. tumida flexuosa* are absent in Unit VI (Samples 942A-8H-CC, 18 cm [70.4 mbsf], through -20X-CC, 37 cm [171.3 mbsf]), and thus this interval has been defined as the Ericson W Zone, penultimate glaciation. Mica, calcareous spines, and fine wood fragments are found in the upper portion of Unit VI (Samples 942A-8H-CC, 18 cm [70.38 mbsf], through -13X-CC, 10–19 cm [108.9 mbsf]). Sand, mica, red and black authigenic mineral nodules, and calcareous spines are present in the lower portion of Unit VI (Samples 942A-15X-CC, 12–21 cm [126.2 mbsf], through -19X-CC, 10–19 cm [165.8 mbsf]). Iron-stained foraminifers occur only at the top of Unit VI (Sample 942A-8H-CC, 18 cm [70.38 mbsf]).

Benthic Foraminifers

Bathyal benthic foraminifers occur only in low abundance in Unit VI (Samples 942A-8H-CC, 18–27 cm [70.4 mbsf], and -13X-CC, 10–19 cm [108.9 mbsf], through -15X-CC, 12–21 cm [126.2 mbsf]), suggesting some reworked component in this unit. Abyssal benthic foraminifers occur in relatively high abundances throughout Hole 942A (Fig. 14).

Siliceous Microfossils

As at previous sites of Leg 155, siliceous microfossils were found only in the mud-line samples of Site 942.

Palynology

Twelve samples were examined from Hole 942A (Table 5). The Y Zone (late Pleistocene) pollen and spore assemblage has very low to moderate abundance and variable preservation, with Gramineae, tricolpate (TC) types, and Cyatheaceae. The X Zone (late Pleistocene) assemblage has very low to moderate abundance and poor preservation, with Cyatheaceae, trilete, and monolete spores present. Poor preservation suggests that older reworked pollen and spores may make a significant contribution to the total palynomorph assemblage in the X Zone samples. The W Zone (middle Pleistocene) assemblage has very low to moderate abundance and poor to moderate preservation with Ericaceae, Cyperaceae, Cyatheaceae, trilete, and monolete spores present. Wood particles were observed in all sample slides in low to moderate abundance (Table 5). Macroscopic wood (>63 μm) was observed in core-catcher samples between 3.86 and 61.04 mbsf (Samples 942A-1H-CC, 12–19 cm; -4H-CC, 15–24 cm; -6H-CC, 35–44 cm; -7H-CC, 3–12 cm). One other core-catcher sample contained macroscopic organic material at 108.90 mbsf (Sample 942A-13X-CC, 10–19 cm). Dinoflagellates are not present.

Stratigraphic Summary

Unit I contains well-preserved nannofossil and planktonic foraminifer assemblages indicative of the Holocene. The nannofossil assemblages represents nannofossil Zone CN15b. The boundary between Ericson Zones Z and Y (disappearance of *G. tumida*) occurs within Unit II between the mud line and 3.77 mbsf. The Ericson Y Zone occurs within Units II and III and contains the 40-ka $Y_{p.obliq.}$ datum at 23 mbsf. The Y Zone has low abundance and variable preservation of spores and pollen. Subunit IIIA nannofossil assemblage contains rare *E. huxleyi*, suggesting that it is older than 85 ka. Units IV and V contain *G. tumida* and *G. menardii* and are defined as the Ericson X Zone, the last interglacial (41.9 to 65.9 mbsf). The nannofossils are from Zone CN15a (85–260 ka). The pollen and spore assemblage contains a high proportion of reworked grains in this interval. Unit VI contains the Ericson W Zone (70.38 to 171.27 mbsf) and low abundances of foraminifers and poorly to moderately preserved spores and pollen. Iron-stained foraminifers at the top of Unit VI and the presence of bathyal benthic foraminifers suggest a reworked component in Unit VI.

PALEOMAGNETISM

Remanence Studies

Archive-half sections from 23 APC cores and eight XCB cores were measured on the pass-through cryogenic magnetometer. Only Core 942B-6H, which was highly disturbed, was not measured. Tensor tool orientations were obtained for Cores 942A-3H through -10H and -12H, Cores 942B-7H and -8H, and Cores 942C-3H through -5H.

Short wavelength oscillations in declination are discernable in limited lengths of core from Holes 942A and 942B, but are best defined in Hole 942C. Ten cycles in 5 m of Hole 942C are numbered in Figure 15. Short wavelength oscillations in inclination are in evidence from 1 to 15 mbsf for Holes 942A, 942B, and 942C. Fourteen cycles that span 7.5 m in Holes 942A and 942B are numbered in Figure 16.

Remanence intensities show high-amplitude variations that can be correlated between holes at this site. A low-intensity zone from ~42 to ~65 mbsf corresponds to Unit IVB, an intensely burrowed dark silty clay interbedded with silty/sandy laminae. The upper part of Unit VI, another dark silty clay with silt laminae, corresponds to a high-remanence intensity zone (Fig. 17).

Two short intervals of anomalous remanence direction and intensity, which could represent geomagnetic excursions, are recorded at

Table 4. Foraminifer abundance data for Holes 942A, 942B, and 942C.

Core, section, interval (cm)	Top interval (mbsf)	Bottom interval (mbsf)	<i>Globorotalia menardii</i>	<i>Globorotalia tumida</i>	<i>Globorotalia tumida flexuosa</i>	<i>Pulleniatina obliquilocutata</i>	<i>Globigerinoides ruber</i> (white)	<i>Globigerinoides ruber</i> (pink)	<i>Globorotalia hexagonus</i>	<i>Neoglobobulimina duterrei</i>	<i>Globorotalia trilobus trilobus</i>	<i>Globorotalia inflata</i>	<i>Globorotalia truncatulinoides</i>	<i>Globigerina bulloides</i>	<i>Globigerinoides trilobus sacculifer</i>	<i>Globorotalia fimbriata</i>	<i>Bolliella adamsi</i>	<i>Hastigerinella digitata</i>	<i>Globigerina calida calida</i>	<i>Globorotalia crassaformis hessi</i>	<i>Globorotalia crassaformis viola</i>	<i>Globorotalia tosaensis</i>	<i>Globorotalia crassaformis crassaformis</i>	Other planktonic foraminifers	Vivianite nodules	Overall foraminifer abundance	Preservation	Abundance of bathyal benthic foraminifers	Abundance of abyssal benthic foraminifers	Comments	Ericson Zone	Age			
155-942A-																																			
1H-MI, 0-0	0.00	0.00	F	C	B	F	C	R	B	C	C	B	B	B	F	R	B	B	B	B	B	B	B	B	A	G	B	R		Z	Holocene				
1H-CC, 12-19	3.68	3.77	B	B	B	C	F	R	B	C	C	B	F	B	F	B	B	B	R	R	B	B	B	B	B	F	M	B	B	W,PT,M	Y	late Pleist.			
2H-CC, 47-56	12.72	12.81	B	B	B	C	F	R	B	C	C	B	F	B	F	B	B	B	R	R	B	B	B	B	B	B	A	G	B	R	SP,PT,BN	Y	late Pleist.		
3H-CC, 18-27	22.94	23.03	B	R	B	F	F	B	B	C	C	B	C	B	F	B	B	B	B	B	B	B	B	B	B	B	C	G	B	C	PT,BN	Y	late Pleist.		
4H-CC, 15-24	32.77	32.86	B	B	B	F	B	R	B	C	C	B	C	B	F	B	B	B	B	B	B	B	B	B	B	B	B	C	G	B	F	M,W	Y	late Pleist.	
5H-CC, 35-44	41.87	41.96	R	A	F	F	F	R	F	C	C	R	R	F	F	B	B	B	B	B	B	B	B	B	B	B	A	G	B	F	SP	X	late Pleist.		
6H-CC, 35-44	51.32	51.41	R	A	F	F	R	B	B	C	C	R	R	F	B	F	B	B	B	B	B	B	B	B	B	B	B	C	G	B	B	M,W	X	late Pleist.	
7H-CC, 3-12	61.04	61.13	R	C	F	F	R	B	B	C	C	B	F	B	F	B	B	B	R	R	B	B	B	B	B	B	F	C	G	B	B	M,W	X	late Pleist.	
8H-4, 60-62	65.90	65.92	C	R	B	F	C	F	B	F	C	B	B	B	F	B	B	B	B	B	B	B	B	B	B	B	A	G	B	B		X	late Pleist.		
8H-CC, 18-27	70.29	70.38	B	B	B	C	F	B	B	C	C	R	F	B	R	B	B	B	B	B	B	B	B	B	B	B	B	F	M	F	R	IS,BN,OS	W	middle Pleist.	
9H-CC, 32-41	77.49	77.58	B	B	B	F	F	B	B	C	C	B	C	B	B	B	B	B	R	R	B	B	B	B	B	B	C	F	G	B	B		W	middle Pleist.	
10H-CC, 32-41	90.00	90.09	B	B	B	F	B	B	B	C	C	B	C	B	C	B	B	B	B	B	B	B	B	B	B	B	A	C	G	B	R	M,SP	W	middle Pleist.	
11H-CC, 19-28	96.86	96.85	B	B	B	B	R	B	B	C	C	B	F	B	C	B	B	B	B	B	B	B	B	B	B	B	B	F	G	B	A		W	middle Pleist.	
12H-CC, 21-30	104.06	104.15	B	B	B	F	B	B	B	C	C	B	C	B	C	B	B	B	B	B	B	B	B	B	B	B	C	R	G	B	C	M	W	middle Pleist.	
13X-CC, 10-19	108.90	108.99	B	B	B	F	B	B	B	C	C	B	C	B	C	B	B	B	B	B	B	B	B	B	B	B	B	A	G	R	R	M,SP,W	W	middle Pleist.	
14X-CC, 11-20	114.71	114.80	B	B	B	C	B	B	B	C	C	B	C	B	F	B	B	B	B	R	B	B	B	B	B	B	B	C	G	B	R		W	middle Pleist.	
15X-CC, 12-21	126.10	126.19	B	B	B	C	B	B	B	C	C	B	C	B	C	B	B	B	B	B	B	B	B	B	B	B	B	A	F	G	R	R	S,RN,SP	W	middle Pleist.
16X-CC, 11-20	135.70	135.79	B	B	B	C	B	B	B	C	C	B	C	B	C	B	B	B	B	B	B	B	B	B	B	B	B	A	F	G	B	F	M	W	middle Pleist.
17X-CC, 11-21	145.40	145.49	B	B	B	F	B	B	B	C	C	B	C	B	C	B	B	B	R	R	B	B	B	B	B	B	B	A	F	G	B	C	M	W	middle Pleist.
18X-CC, 9-18	156.04	156.13	B	B	B	F	B	B	B	C	C	B	C	B	R	B	B	B	B	B	B	B	B	B	B	B	B	C	F	G	B	F		W	middle Pleist.
19X-CC, 10-19	165.71	165.80	B	B	B	B	B	B	B	B	B	B	B	B	B	B	B	B	B	B	B	B	B	B	B	B	B	C	B	B	B	S		W	middle Pleist.
20X-CC, 28-37	171.18	171.27	B	B	B	R	B	B	B	A	F	B	C	B	B	B	B	B	B	B	B	B	B	B	B	B	B	A	R	G	B	B	M,BN	W	middle Pleist.
155-942B-																																			
1H-CC, 12-21	7.35	7.44	B	B	B	C	F	F	B	C	A	B	R	B	A	B	B	B	R	R	B	B	B	B	B	B	A	G	F	B	BN,SP,PT	Y	late Pleist.		
2H-CC, 9-18	16.85	16.94	B	B	B	F	C	F	B	C	C	B	C	B	F	B	B	B	B	R	B	B	B	B	B	B	B	A	G	F	B	PT,BN	Y	late Pleist.	
3H-CC, 0-9	26.00	26.09	B	B	B	R	R	B	B	R	F	B	R	B	B	B	B	B	B	B	B	B	B	B	B	B	B	R	M	B	B	S,M,FO	Y	late Pleist.	
4H-CC, 11-20	36.19	36.28	F	F	R	C	C	R	B	B	C	C	R	F	B	R	B	B	B	B	B	B	B	B	B	B	B	C	G	F	R	M,BN,OS	X	late Pleist.	
6H-CC, 2-11	46.61	46.70	B	F	B	F	F	R	B	C	C	R	C	B	C	B	B	B	B	R	B	B	B	B	B	B	B	C	G	B	B	M,FO,BN	X	late Pleist.	
7H-CC, 18-27	64.68	64.77	B	C	F	C	C	B	B	F	C	R	B	B	F	B	B	B	B	B	B	B	B	B	B	B	B	R	C	G	B	B	M,SP	X	late Pleist.
8H-CC, 25-34	74.58	74.67	B	B	B	B	R	B	B	B	C	F	F	C	B	R	B	B	B	B	B	B	B	B	B	B	B	F	C	M	F	R	IS,OS,BN	W	middle Pleist.
155-942C-																																			
1H-CC, 3-12	4.20	4.29	R	B	B	C	F	R	R	B	F	C	R	C	B	C	B	B	B	B	B	B	B	B	B	B	B	C	G	R	B	FO,M	Z	Holocene	
2H-CC, 11-20	13.92	14.01	B	B	B	C	F	R	R	C	C	R	C	B	F	B	B	B	B	B	B	B	B	B	B	B	B	C	G	R	B	BN,SP,OS,PT,SF	Y	late Pleist.	
3H-CC, 0-7	45.66	45.73	R	C	R	C	F	R	R	C	C	F	R	F	B	B	B	B	B	B	B	B	B	B	B	B	B	C	G	B	B	M,BN	X	late Pleist.	
4H-CC, 27-36	55.40	55.49	R	F	R	C	F	R	R	C	F	B	F	B	F	B	B	B	B	B	B	B	B	B	B	B	B	F	G	B	B	M	X	late Pleist.	
5H-CC, 12-21	72.17	72.26	B	F	R	B	F	B	B	B	C	F	B	C	B	F	B	B	B	B	B	B	B	B	B	B	B	F	F	M	R	F	IS,BN,SP,OS	X	late Pleist.

Notes: Key to Comments section: Sediment composition: PT = pteropods, S = sand, M = mica, BN = black nodules, RN = red nodules; indicators of reworking: SF = shell fragments, FO = fine organics, W = wood fragments, OS = ostracod shells, SP = sponge spicules or spines, IS = iron-stained foraminifers. Note also the occurrence of bathyal benthic foraminifers.

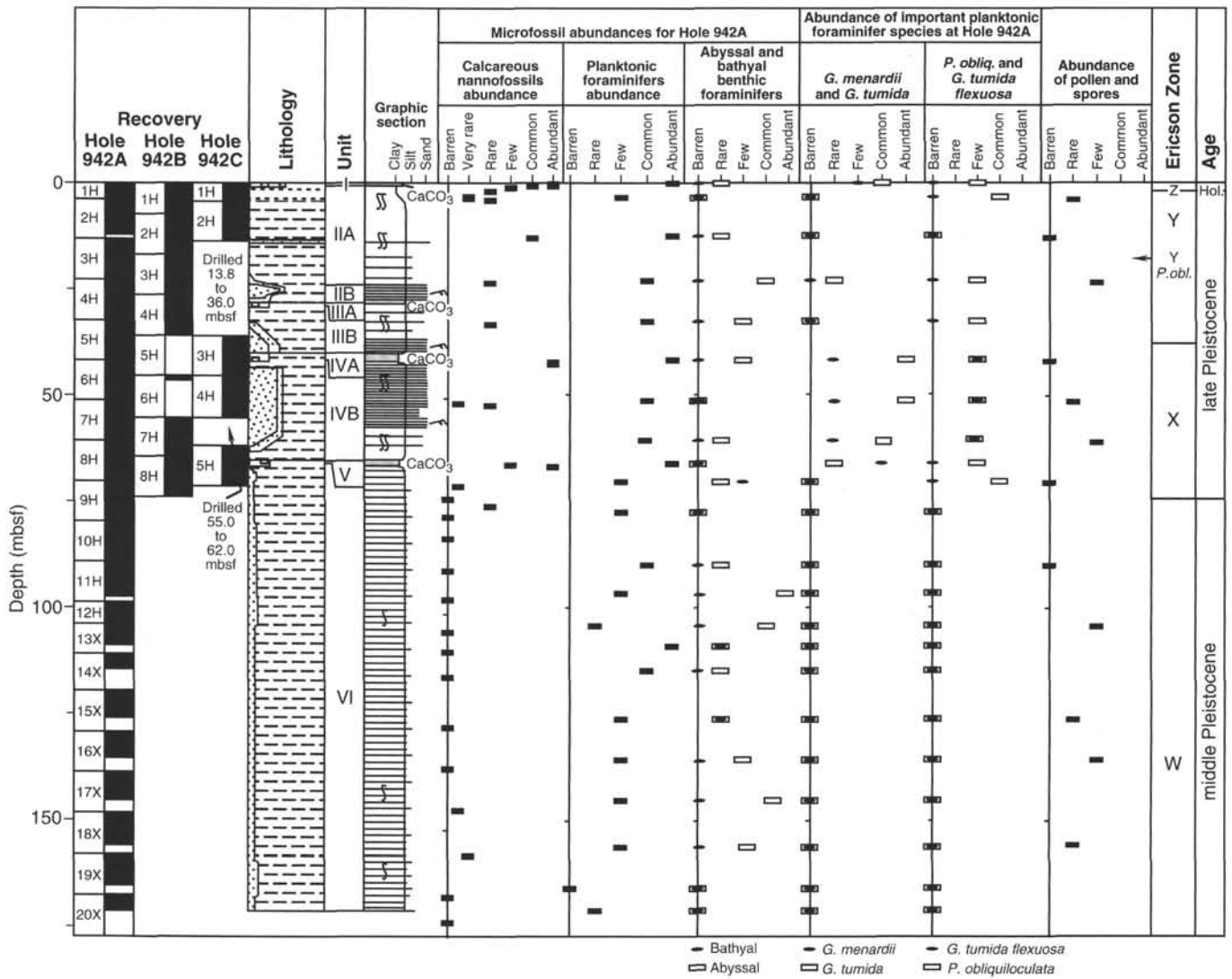


Figure 14. Biostratigraphic summary for Site 942.

Table 5. Spores and pollen data for Hole 942A.

Core, section, interval (cm)	Top interval (mbsf)	Bottom interval (mbsf)	Pollen and spores			Dinocysts	Wood/ carbonized particles	Ericson Zone (inferred from forams)	Age (inferred from forams)
			Abundance	Preservation	Major types recorded				
155-942A-									
1H-CC, 21-22	3.77	3.78	r	p	Cyatheaceae	b	f	Y	late Pleist.
2H-CC, 56-57	12.81	12.82	b			b	r	Y	late Pleist.
3H-CC, 27-28	23.03	23.04	f	g	Gramineae, tricolpate	b	f	Y	late Pleist.
5H-CC, 44-45	41.96	41.97	b			b	f	X	late Pleist.
6H-CC, 44-45	51.41	51.42	r	p	Trilete spore	b	f	X	late Pleist.
7H-CC, 12-13	61.13	61.14	f			b	f	X	late Pleist.
8H-CC, 27-28	70.38	70.39	b			b	f	W	middle Pleist.
10H-CC, 41-42	90.09	90.10	b			b	f	W	middle Pleist.
12H-CC, 30-31	104.15	104.16	f	p	Cyperaceae, Cyatheaceae	b	f	W	middle Pleist.
15X-CC, 21-22	126.19	126.20	r	m	Monolete spore	b	f	W	middle Pleist.
16X-CC, 20-21	135.79	135.80	f	m	Ericaceae, trilete spore	b	c	W	middle Pleist.
18X-CC, 18-19	156.13	156.14	r	m	Monolete spore	b	f	W	middle Pleist.

this site. The first occurs in Section 942A-2H-7, between 11 and 12 mbsf, and Section 942C-2H-4, between 9 and 10 mbsf. Its characteristics in Hole 942A are similar to those of the Lake Mungo Excursion, consisting of a rapid shift of inclination to high positive values accompanied by an increase in remanence intensity. In Hole 942C the inclination signal is somewhat distorted, but a rapid shift toward pos-

itive values is recorded at ~9.5 mbsf (Fig. 16). In Hole 942B, these changes in remanence are inexplicably absent.

The second anomalous region overlaps with carbonate-rich Unit IVA in Sections 942A-5H-7 and -6H-1 (41.0 to 42.2 mbsf), and in Section 942C-3H-2 (37.5 to 38.7 mbsf). Its characteristic features are a series of closely spaced oscillations in declination and a shift to high

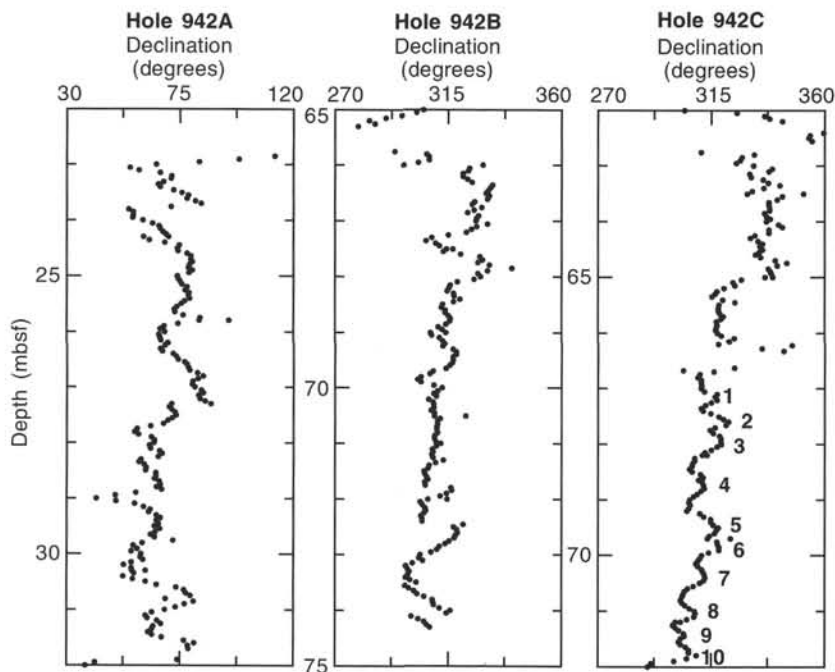


Figure 15. Azimuthally corrected declinations over selected intervals for Holes 942A, 942B, and 942C. Sequential cycles are numbered 1–10 for Hole 942C. AF demagnetization level was 20 mT. No correlation between holes at these intervals is implied.

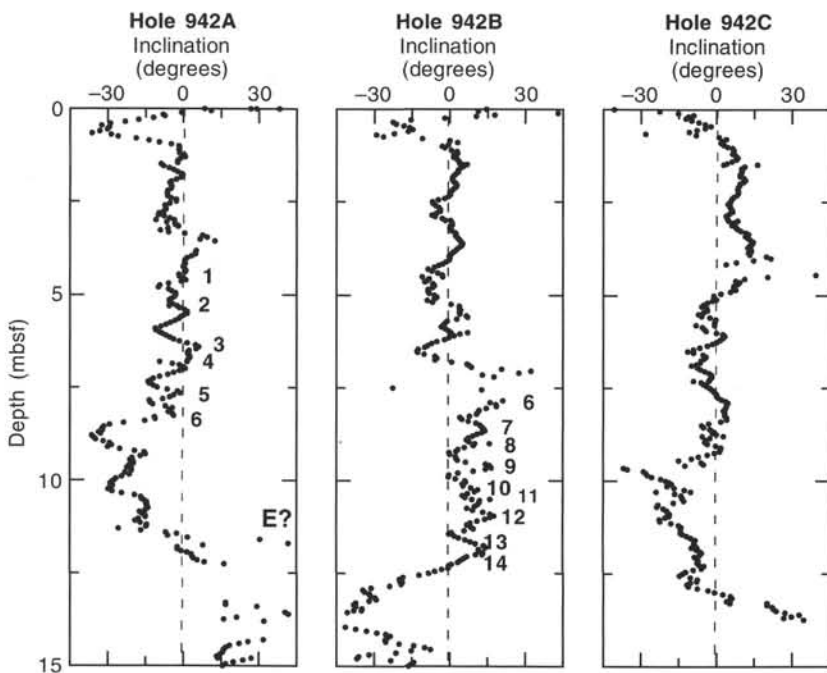


Figure 16. Inclinations for a depth of 0–15 mbsf for Holes 942A, 942B, and 942C. Sequential cycles are numbered 1–6 in Hole 942A and 6–14 in Hole 942B. “E” refers to a high positive inclination zone that possibly represents the Lake Mungo geomagnetic excursion (~30 ka). AF demagnetization level was 20 mT. Note that ~4 m of Hole 942C sediment is missing immediately below ~4 mbsf (see Fig. 21).

positive inclinations, accompanied by a decrease in remanence intensity (Fig. 18). The top of this probable excursion could not be determined from the archive-half measurements because a portion of the core liner for the overlying Section 942C-3H-1 was flattened and would not fit into the track of the pass-through magnetometer. However, over 100 discrete 1-cm³ samples were taken from the working halves of these sections for post-cruise remanence analyses.

A comparison of remanence intensity, after AF demagnetization to 20 mT, in the top 15 m of Holes 942A and 942C shows the relationship between the upper excursion and intensity peaks A–E (Fig. 19). Peak B is missing in Hole 942C due to the loss of ~4 m of sediment immediately below Core 942C-1H at ~4 mbsf (see below). When this offset is taken into consideration, the intensity features

maintain their same relative position with respect to the Lake Mungo Excursion (~30 ka) in the previous levee sites (e.g., Fig. 15, “Site 933” chapter, this volume). The deeper anomalous remanence zone, which was stratigraphically correlative in Holes 942A and 942C (the equivalent depth in Hole 942B had no recovery), may correspond to the Blake geomagnetic event (~105 ka).

Magnetic Susceptibility Studies

Whole-core magnetic susceptibility was measured on all cores collected from Site 942. Discrete samples were measured for Hole 942A. No discrete samples were collected within carbonate units because of their importance to micropaleontological and isotopic stud-

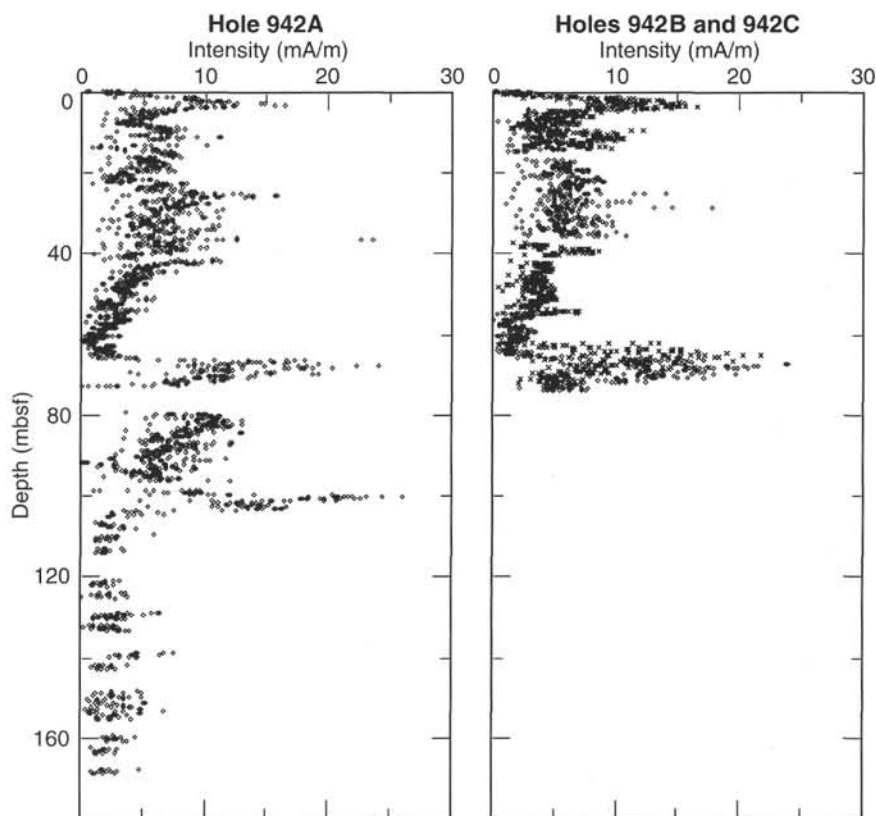


Figure 17. Comparison of remanence intensities for Hole 942A vs. 942B and 942C. Hole 942C values are plotted as x's. AF demagnetization level was 20 mT. Note that ~4 m of Hole 942C sediment is missing immediately below ~4 mbsf (see Fig. 21).

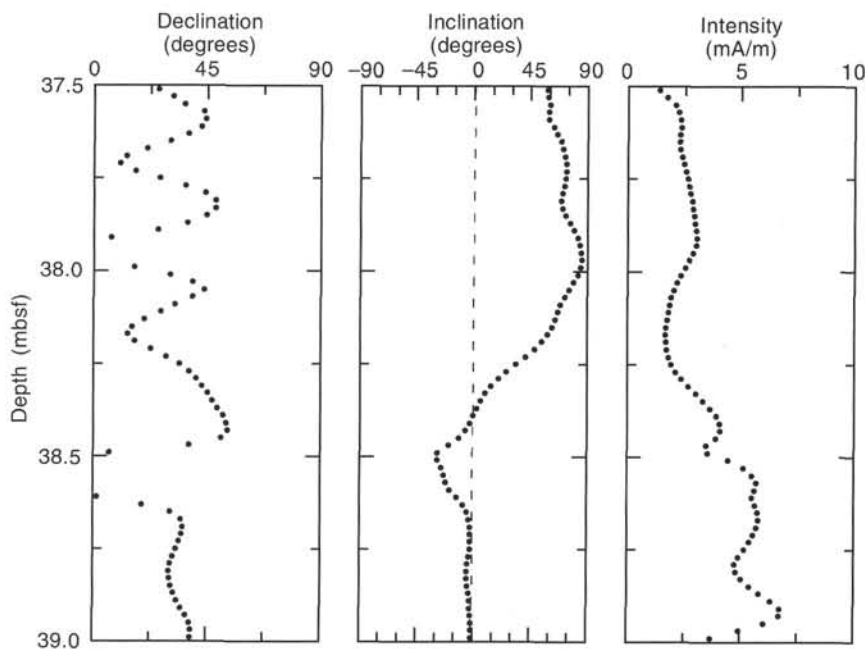


Figure 18. Uncorrected declination, inclination, and remanence intensity over a 1.5-m interval of Hole 942C, which may represent the Blake Event (~105 ka). AF demagnetization level was 25 mT.

ies. The results from Hole 942A are used to represent the site (Fig. 20).

The lowest susceptibility values are found within the carbonate-rich Unit V. This reflects the finer grain size of its sediment coupled with increased biogenic dilution of the magnetic mineral concentration.

In addition, we present a preliminary correlation scheme for this site based on the comparison of the susceptibility data for the three

holes (Fig. 21). These comparisons show that, with respect to Hole 942A, the tie points of Hole 942B occur at about the same depths (within 1 m). However, the tie points within Hole 942C are about 4 m shallower than those of Hole 942A. This is consistent with the lithologic correlation (see "Lithostratigraphy" section, this chapter). The correlation pattern suggests the offset begins at the boundary between Cores 942C-1H and -2H, and continues downhole (see "Operations" section, this chapter). For Holes 942A and 942B, we see a

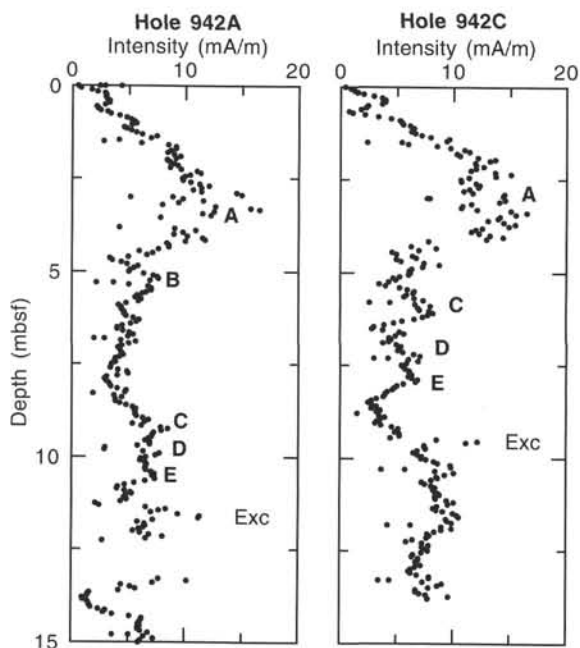


Figure 19. Comparison of remanence intensities, after AF demagnetization to 20 mT, between Holes 942A and 942C, for 0–15 mbsf. “Exc” denotes apparent position of Lake Mungo Excursion (~30 ka). A–E are intensity peaks seen in previous levee sites (Fig. 15 of “Site 933” chapter, this volume). Note that ~4 m of Hole 942C sediment is missing immediately below ~4 mbsf (see Fig. 21).

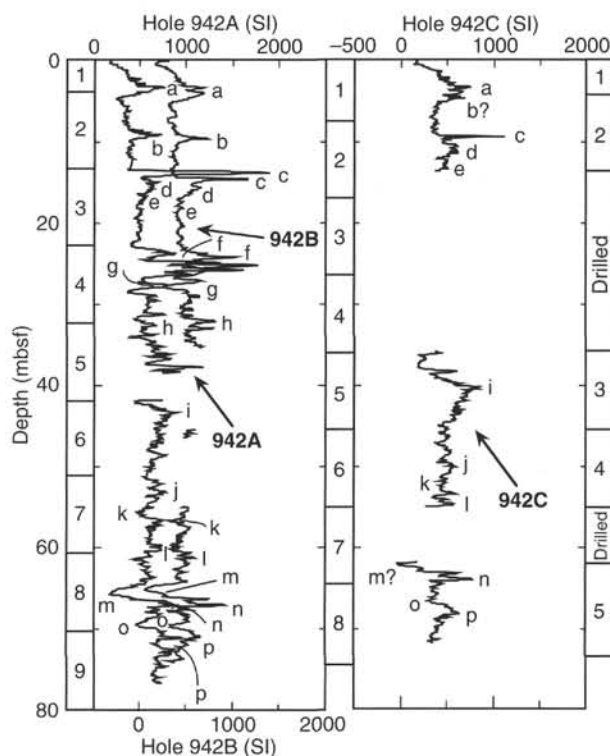


Figure 21. Preliminary correlation between holes for Site 942 based on the whole-core magnetic susceptibility records. The core numbers are written in boxes outside the figure.

4-m region of relatively low susceptibility between tie-points a and b, which may be missing in Hole 942C.

ORGANIC GEOCHEMISTRY Volatile Hydrocarbons

Headspace methane concentrations increase rapidly below the sediment surface to a maximum value of 57,218 ppm at 31.80 mbsf (Table 6; Fig. 22). Below 50.80 mbsf methane concentrations remain fairly constant, ranging from 6,200 ppm to 15,200 ppm. Vacutainer methane values are considerably higher than headspace concentrations (Fig. 22), ranging from 50,000 ppm at 50.80 mbsf to ~600,000 ppm at 82.80 mbsf. Higher molecular weight hydrocarbons were not found, indicating a predominantly biogenic methane source at Site 942.

Carbon, Nitrogen, and Sulfur Concentrations

The majority of samples for elemental analysis were taken from Hole 942A, with three additional samples collected from Hole 942B and one from Hole 942C. Holes 942B and 942C displayed discrepancies in reported drilling depths relative to Hole 942A (see “Operations” section, this chapter; Table 7). For graphic representation of the data (Fig. 23), these reported depths were shifted to agree with the Hole 942A depths based on magnetic susceptibility and lithologic correlations. Only reported depths, however, are used in the following discussion.

Carbonate (calculated as CaCO₃) concentrations are low (≤4.0%) between 1.56 and 26.49 mbsf and below 86.46 mbsf (Table 7; Fig. 23). In Hole 942A, a slightly elevated carbonate content was found at 27.33 mbsf (4.5%) and high values were observed at 40.55 mbsf

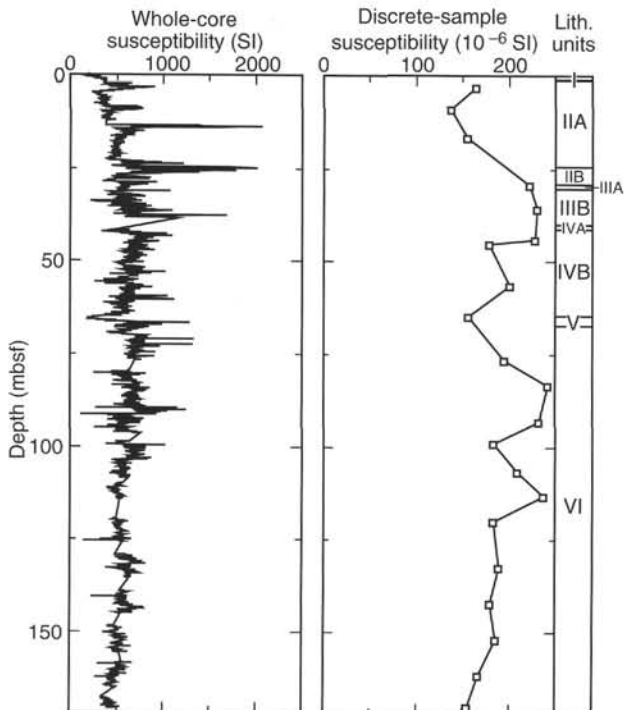


Figure 20. Whole-core and discrete-sample magnetic susceptibilities for Site 942.

Table 6. Gas concentrations in sediment from Site 942.

Core, section, interval (cm)	Depth (mbsf)	Sed. temp.* (°C)	Methane	
			HS (ppm)	VAC (ppm)
155-942A-				
1H-2, 0-5	1.50	2	6	
2H-6, 0-5	9.80	2	17	
3H-5, 0-5	19.30	3	27,291	
4H-7, 0-5	31.80	3	57,218	
5H-4, 0-5	40.09	3	27,136	
6H-7, 12-17	50.80	3	9,942	49,569
7H-7, 0-5	60.30	4	6,448	176,263
8H-7, 0-5	69.80	4	9,390	476,088
10H-4, 0-5	82.80	4	7,954	598,168
11H-6, 0-5	95.43	5	8,358	507,045
12H-3, 0-5	101.59	5	9,313	
13X-3, 0-5	107.00	5	15,152	
14X-3, 0-5	113.10	5	7,680	
15X-3, 0-5	122.70	5	6,180	
17X-4, 0-5	143.50	6	9,218	
18X-5, 0-5	154.60	6	6,750	
19X-3, 0-5	161.30	7	8,139	

Notes: HS = headspace; VAC = vacutainer. Geothermal gradient = 38°C/km. Bottom-water temperature = 2°C. *See "In-situ Temperature Measurements" section, this chapter.

(9%), 73.46 mbsf (16%), and 82.54 mbsf (14%). In addition, high carbonate concentrations ranging from 12% to 32% were observed in several samples from Holes 942B and 942C at depths of 27.98 mbsf and 62.00 to 65.70 mbsf. The high carbonate values at ~28, ~41, and ~65 mbsf correspond to foraminifer-nannofossil-rich lithologic Units IIIA, IVA, and V, respectively. On the other hand, the two high carbonate values at 73.46 mbsf and 82.54 mbsf, which are measured in samples from the top of turbidites, are composed of diagenetic siderite.

Table 7. Elemental and organic carbon compositions of sediment from Site 942.

Core, section interval (cm)	Depth (mbsf)	IC (%)	CaCO ₃ ^a (%)	TC (%)	TOC (%)	TN (%)	TS (%)	[C/N] ^a	Depth ^b (mbsf)
155-942A-									
1H-2, 6-7	1.56	0.17	1.4	0.98	0.81	0.10	0.37	10	
2H-4, 37-38	8.67	0.36	3.0	1.14	0.78	0.08	0.13	11	
3H-4, 36-37	18.16	0.38	3.2	1.04	0.66	0.08	0.12	10	
4H-3, 69-70	26.49	0.18	1.5	0.90	0.72	0.07	0.06	11	
4H-4, 3-4	27.33	0.54	4.5	1.09	0.55	0.08	0.11	8	
5H-1, 47-49	32.77	0.21	1.7	0.70	0.49	0.06	0.06	9	
5H-7, 46-47	40.55	1.04	8.7	1.68	0.64	0.08	0.09	9	
6H-1, 46-47	42.26	0.17	1.4	0.54	0.37	0.06	0.07	7	
6H-5, 140-141	49.20	0.24	2.0	0.62	0.38	0.07	0.05	7	
7H-4, 115-116	56.95	0.10	0.8	0.12	0.02	0.01	0.07	3	
7H-6, 5-6	58.85	0.18	1.5	0.65	0.47	0.09	0.06	6	
8H-5, 55-56	67.35	0.09	0.7	0.66	0.57	0.11	0.14	6	
8H-6, 119-120	69.49	0.25	2.1	1.02	0.77	0.11	0.47	8	
9H-4, 79-80	73.46	1.97 ^c	16.4	2.77	0.80	0.10	0.10	9	
9H-7, 12-13	75.55	0.46	3.8	1.28	0.82	0.09	0.08	10	
10H-2, 124-125	82.54	1.71 ^c	14.2	2.37	0.66	0.08	0.03	10	
10H-5, 66-67	86.46	0.29	2.4	1.08	0.79	0.10	0.04	9	
11H-5, 4-5	93.97	0.47	3.9	1.40	0.93	0.11	0.05	10	
12H-3, 51-52	102.10	0.40	3.3	1.33	0.93	0.11	0.05	10	
13X-3, 58-59	107.58	0.32	2.7	1.33	1.01	0.11	0.04	10	
14X-2, 39-40	111.99	0.26	2.2	1.29	1.03	0.12	0.07	10	
15X-3, 47-48	123.17	0.27	2.2	1.28	1.01	0.11	0.00	11	
16X-4, 76-77	134.56	0.30	2.5	1.31	1.01	0.11	0.05	11	
17X-4, 79-80	144.29	0.29	2.4	1.30	1.01	0.12	0.00	10	
18X-4, 53-54	153.63	0.29	2.4	1.37	1.08	0.12	0.04	10	
19X-4, 36-37	163.16	0.28	2.3	1.33	1.05	0.10	0.04	12	
20X-2, 42-43	169.82	0.23	1.9	1.29	1.06	0.11	0.03	11	
155-942B-									
4H-2, 148-150	27.98	1.70	14.2	2.13	0.43	0.06	0.06	8	28.85
8H-2, 80-90	65.30	3.14	26.2	3.54	0.40	0.07	0.09	7	65.85
8H-2, 120-125	65.70	1.50	12.5	1.84	0.34	0.07	0.04	6	66.08
155-942C-									
5H-2, 1-10	62.00	3.81	31.7	4.07	0.26	0.06	0.00	5	65.55

^aCalculated assuming all IC is calcite.

^bDepths from Holes 942B and 942C were shifted to fit the depth scale of Hole 942A using magnetic susceptibility and lithologic correlations (see "Paleomagnetism" and "Lithostratigraphy" sections, this chapter).

^cSample contains iron carbonate, siderite, not calcium carbonate (see "Inorganic Geochemistry" section, this chapter).

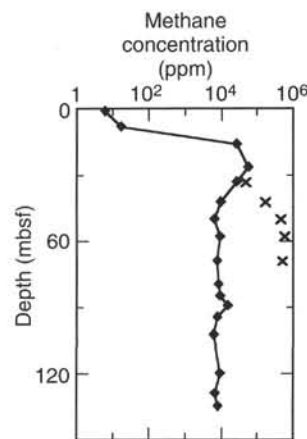


Figure 22. Methane concentrations at Site 942. Headspace (diamond) and vacutainer (x) samples are plotted.

Elemental composition differences from previous sites are also obvious in the TOC concentration profile in Hole 942A. TOC values are ~0.8% in the dark gray clay at 1.56 and 8.67 mbsf. Below 8.67 mbsf, the TOC concentrations steadily decrease to values lower than 0.5% between 42.26 and 58.85 mbsf. A very low TOC value (0.02%) was detected in an interval of fine sand at 56.95 mbsf. Below 58.85 mbsf, TOC values increase to slightly higher than 1% at 107.58 mbsf and remain fairly constant to the bottom of the hole.

Total nitrogen concentrations at this site show a profile similar to that of TOC. The values range between 0.06% and 0.12%. A very low value (0.01%) was detected in a fine sand layer at 56.95 mbsf. In general, total sulfur concentrations are low (<0.15%) throughout Site

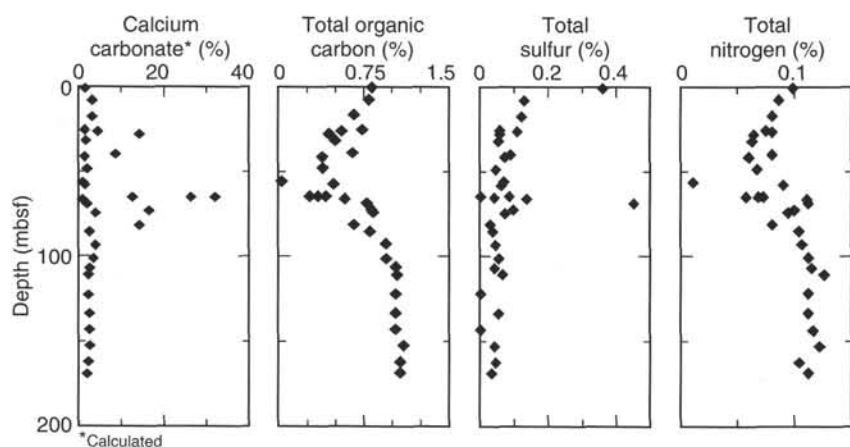


Figure 23. Concentration profiles of carbonate, total organic carbon, total sulfur, and total nitrogen at Site 942. The depths for the calcium carbonate data from Holes 942B and 942C were shifted to fit those from Hole 942A based on paleomagnetic and lithostratigraphic correlations.

942. Slightly elevated concentrations (0.37% and 0.47%) were observed at the tops of lithologic Unit II (1.56 mbsf) and Unit VI (69.49 mbsf). The [C/N]a ratios generally range from 6 to 12 with the lowest values (6 to 9) between 27.33 mbsf and 73.46 mbsf.

The interval between ~28.55 mbsf and ~66.08 mbsf, which represents Ericson Zone X, is characterized by an elemental composition different from that of the rest of Site 942. This interval shows three peaks of high carbonate content that probably represent hemipelagic deposition periods during sea level highstands. The TOC concentrations in this interval are similar to those of Holocene fan sediment. The elevated TS concentration below the Ericson Zone X is also similar to the higher TS values observed below the Holocene intervals at previous sites. Both of these features likely reflect iron sulfide precipitation as a result of sulfate reduction. The [C/N]a ratios in this interval are consistently lower than those of the rest of Site 942, suggesting a different organic matter composition.

INORGANIC GEOCHEMISTRY

Interstitial Water Analysis

Interstitial waters were analyzed from nine sediment samples at Hole 942A. Samples were taken approximately every 10 m for the upper 35 mbsf and approximately every 30 m thereafter to a depth of 169.30 mbsf (Table 8; Fig. 24).

Salinities of the water samples range from 32.0 to 35.0 (Fig. 24A). The salinity decreases from 35.0 near the sediment surface to 32.5 at 19.25 mbsf. From 19.25 mbsf to near the bottom of the hole, the salinities fall into two distinct groups. In the interval 19.25–69.70 mbsf, the salinity is comparatively low, varying between 32.0 and 32.5. In the interval 95.33–169.30 mbsf, the salinity is higher, ranging from 33.5 to 34.0. The transition from lower to higher salinities occurs at approximately the transition from Ericson Zone X to W (approximately equivalent to the transition from interglacial Stage 5 to glacial

Stage 6; see “Biostratigraphy” section, this chapter). The salinity changes parallel changes in concentrations of calcium and magnesium throughout the hole, and below 9.75 mbsf are roughly similar to changes in iron, alkalinity, and ammonium.

Chloride concentrations range from 552 to 559 mM. The concentration increases from 552 mM at 1.45 mbsf to 559 mM at 19.25 mbsf (Fig. 24B). Below 19.25 mbsf, the chloride concentration is fairly constant, ranging from 556 to 559 mM downhole.

Pore-water pH values are between 7.69 and 7.59 in the upper 19.25 mbsf, increasing slightly to 7.74–7.77 over the interval 31.75–95.33 mbsf, and decreasing again to between 7.43 and 7.55 in the three deepest samples, from 113.00 mbsf and below (Fig. 24C). The pore-water pH profile is almost a mirror image of the salinity profile and also varies inversely with alkalinity, magnesium, and calcium. These relationships suggest that pH, alkalinity, calcium, and magnesium concentrations are controlled by equilibrium with a carbonate mineral.

Alkalinity values increase rapidly in the upper few meters of the hole, from 7.13 mM at 1.45 mbsf to 26.07 mM at 9.75 mbsf (Fig. 24D). The values then decrease to 11.07 mM at 35.25 mbsf and remain at about 10 mM through 95.33 mbsf. Alkalinity increases again to a second peak of 30.31 mM at 143.40 mbsf, and decreases to 16.88 mM in the lowermost sample.

Magnesium and calcium concentrations closely parallel each other. The concentrations decrease from 51.7 mM magnesium and 10.6 mM calcium at 1.45 mbsf to 40.6 mM magnesium and 5.2 mM calcium at 35.25 mbsf (Fig. 24E and 24F). The concentrations remain near these values to 95.33 mbsf, then increase to about 46 mM magnesium and 7 mM calcium from 113.00 to 143.30 mbsf. The values decrease again to 41.4 mM magnesium and 5.6 mM calcium in the lowermost sample.

Pore-water sulfate concentrations decrease from 25.3 mM at 1.45 mbsf to 5.5 mM at 9.75 mbsf to zero by 19.25 mbsf (Fig. 24G). Below 19.25 mbsf, sulfate concentrations generally remain at or near

Table 8. Interstitial water chemistry, Site 942.

Core, section, interval (cm)	Depth (mbsf)	Salinity	pH	Alkalinity (mM)	Cl ⁻ (mM)	Mg ²⁺ (mM)	Ca ²⁺ (mM)	K ⁺ (mM)	HPO ₄ ²⁻ (μM)	SO ₄ ²⁻ (mM)	NH ₄ ⁺ (mM)	H ₄ SiO ₄ (μM)	Na ⁺ (mM)	Fe ²⁺ (μM)	Mn ²⁺ (μM)
155-942A-															
1H-1, 145–150	1.45	35.0	7.69	7.13	552	51.7	10.6	12.8	21.7	25.3	0.6	356	472	43.1	56.4
2H-4, 145–150	9.75	34.0	7.59	26.07	556	45.8	8.2	11.7	46.9	5.5	1.7	335	471	77.4	45.6
3H-4, 145–150	19.25	32.5	7.61	23.79	559	43.2	6.7	10.5	16.7	0.3	2.4	256	471	91.6	7.2
4H-6, 145–150	31.75	32.5	7.75	14.35	556	41.6	5.6	9.7	64.0	0.2	2.8	363	464	76.4	3.2
5H-2, 145–150	35.25	32.5	7.77	11.07	558	40.6	5.2	10.0	21.7	0.6	3.6	361	465	44.1	3.2
8H-6, 140–150	69.70	32.0	7.74	9.70	559	39.0	5.0	8.7	13.3	0.4	6.9	356	466	10.3	10.0
11H-5, 140–150	95.33	33.5	7.77	13.21	557	40.2	5.2	7.4	9.9	0.1	9.8	443	462	39.6	2.4
14X-2, 140–150	113.00	34.0	7.55	20.98	557	45.3	6.7	7.8	4.0	4.1	10.7	394	463	66.8	4.4
17X-3, 140–150	143.40	34.0	7.43	30.31	556	46.4	7.0	7.6	0.0	1.6	12.0	489	463	42.9	4.8
20X-1, 140–150	169.30	33.5	7.52	16.88	559	41.3	5.6	7.8	10.7	0.8	12.4	546	463	60.8	2.8

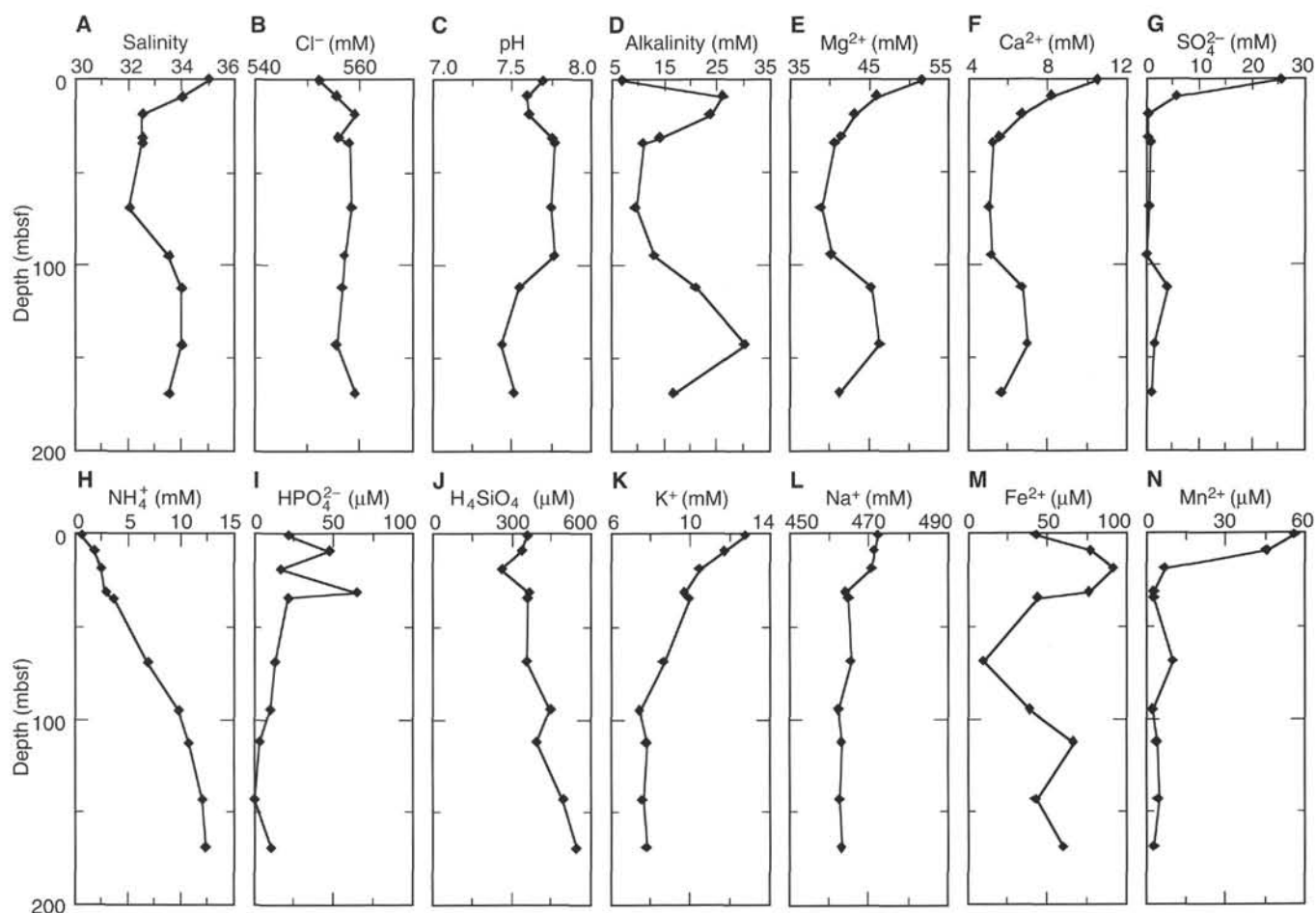


Figure 24. Downhole variation in pore-water chemistry. A. Salinity. B. Chloride. C. pH. D. Alkalinity. E. Magnesium. F. Calcium. G. Sulfate. H. Ammonium. I. Phosphate. J. Silica. K. Potassium. L. Sodium. M. Iron. N. Manganese.

zero for the remainder of the hole. Sampling artifacts produced values above zero at 113.00 and 143.40 mbsf (4.1 and 1.6 mM).

The initial increase in ammonium concentration with depth is slow compared to that at previous sites from this leg. The values increase from 0.6 mM at 1.45 mbsf to 3.6 mM at 35.25 mbsf (Fig. 24H). Below 35.25 mbsf, the ammonium concentration increases more rapidly to 9.8 mM and continues to increase, reaching 12.4 mM near the bottom of the hole.

The pore-water phosphate concentrations in the upper part of the core are more variable than those at previous sites. Two concentration peaks, 46.9 μM at 9.75 mbsf and 64.0 μM at 31.75 mbsf, are observed (Fig. 24I). Outside of these two samples, concentrations generally range from 10 to 20 μM .

Dissolved silica concentrations range from 256 to 546 μM (Fig. 24J). The concentrations generally increase downhole, with the maximum concentration near the bottom of the hole.

Potassium and sodium concentrations show similar downhole profiles (Fig. 24K and 24L). The concentrations decrease from 12.8 mM potassium and 472 mM sodium at 1.45 mbsf to 7.4 mM potassium and 462 mM sodium at 95.33 mbsf. The concentrations remain at those levels downhole.

Dissolved iron concentrations increase from 43.1 μM at 1.45 mbsf to a peak of 91.6 μM at 19.25 mbsf (Fig. 24M). The concentration then decreases to a minimum of 10.3 μM at 69.70 mbsf. Below 69.70 mbsf, the concentrations increase again, ranging from 39.6 to 66.8 μM .

Manganese concentrations decrease sharply from a maximum of 56.4 μM at 1.45 mbsf to 7.2 μM at 19.25 mbsf. Below this depth, the concentrations remain below 10 μM downhole.

Diagenetic siderite was identified from several carbonate-rich layers in Hole 942A (Samples 942A-9H-4, 79–80 cm, and 942A-10H-2, 124–125 cm).

Overall, the pore-water chemistry at this site shows distinct, although minor, differences between the water in the sediment from above vs. that below approximately 100 mbsf. The major lithologic difference in the sediment above and below this level appears to be a decrease in the number of thin sand layers in the deeper sediment of Unit VI (see "Lithostratigraphy" section, this chapter).

Sediment Geochemistry

Four mud samples from an old levee on the western edge of the fan were analyzed for major- and trace-element geochemistry (Tables 9 and 10), and have compositions that are within range of those for previous sites. SiO_2 varies from 61 to 65 wt%, and Al_2O_3 between 20 and 22 wt%. CaO abundances in three muds are between 0.8 and 0.9 wt%, indicating a dominantly silicate mineralogy. The mud with 1.1 wt% CaO (39.18 mbsf) was sampled near a carbonate-rich layer, and thus likely has a higher carbonate content than other muds. This mud also has high SiO_2 and lower abundances of other elements (e.g., Al_2O_3 , Fe_2O_3 , P_2O_5). This probably reflects dilution of clay components by a coarser detrital component.

Table 9. Major element composition (wt%) of sediment samples, Site 942.

Core, section, interval (cm)	Depth (mbsf)	Lithology	SiO ₂	TiO ₂	Al ₂ O ₃	Fe ₂ O ₃	MnO	MgO	CaO	Na ₂ O	K ₂ O	P ₂ O ₅	Total	LOI
155-942A-														
5H-6, 59-62	39.18	Mud	64.95	0.96	19.59	6.98	0.08	1.80	1.13	1.38	2.81	0.13	99.81	7.00
9H-5, 50-53	74.67	Mud	61.32	1.06	21.70	8.22	0.14	2.15	0.78	1.51	3.15	0.18	100.22	8.10
15X-4, 55-58	124.75	Mud	61.14	1.10	22.37	8.20	0.12	2.24	0.82	1.55	3.08	0.21	100.83	8.57
20X-2, 78-83	170.18	Mud	60.97	1.09	22.19	8.25	0.14	2.17	0.87	1.50	2.98	0.18	100.32	8.36

Notes: Total iron is reported as Fe₂O₃. LOI = loss on ignition.

Table 10. Trace element composition (ppm) of sediment samples, Site 942.

Core, section, interval (cm)	Depth (mbsf)	Lithology	Ba	Ce	Cr	Cu	Nb	Ni	Rb	Sr	V	Y	Zn	Zr
155-942A														
5H-6, 59-62	39.18	Mud	455	98	62	26	20	31	125	153	82	36	111	247
9H-5, 50-53	74.67	Mud	502	113	71	35	22	36	136	144	90	39	128	230
15X-4, 55-58	124.75	Mud	509	108	69	35	22	37	132	146	93	40	133	225
20X-2, 78-83	170.18	Mud	497	108	67	34	22	36	126	149	88	38	127	215

PHYSICAL PROPERTIES

Index Properties

Index properties were measured on intact, predominantly clayey sediment intervals in Hole 942A (Table 11). The foraminifer-nannofossil clay of lithologic Unit I was not sampled for index property measurements. Within the silty clay of Unit II, water content decreases from 61% near the seafloor to 39% at 27 mbsf (Fig. 25). Water contents lower than the general trend do not correlate with specific physical features and may be associated with the relatively abundant and large burrows in Unit II. Water content is above the general trend at 28.35 mbsf in Subunit IIIA. Subunit IIIB has a scatter of water content values similar to Unit II (Fig. 25). Samples near the top of Subunit IIIB, at 29.66 mbsf and 31.25 mbsf, have low water contents of 31.2% and 29.5%, respectively. These samples were taken close to sand layers and may have undergone enhanced pore-water drainage.

Subunit IVA, like Subunit IIIA, has a water content higher than the general trend. Water content in the upper part of Subunit IVB shows a scatter similar to that noted in Subunits IIA, IIB, and IIIB. Below 53 mbsf the variability of water content in Subunit IVB is reduced (Fig. 25). Water content increases at the base of the unit, in response to a reduction in silt laminae or possibly an increase in calcareous constituents. The foraminifer-nannofossil clay of lithologic Unit V was not sampled.

Water content decreases from 35% at the top of the terrigenous silty clay of Unit VI to 28% at the base of Hole 942A (Fig. 25). The change in coring methods from APC to XCB at 104 mbsf is clearly shown in the water content profile. All the cores display distinct 1.5% to 3.5% decreases in water content over the length of each core. This pattern occurs at other Leg 155 sites, most notably Sites 932 and 937, and has been attributed to sediment expansion in the core barrel during coring.

Grain density averages 2.74 g/cm³ in Hole 942A, with most of the values between 2.7 to 2.8 g/cm³ (Table 11). There is no obvious explanation for the anomalously high grain densities (2.8–2.9 g/cm³) of some samples at the base of Unit IV and top of Unit VI. Because of the low overall variability of grain density, downhole variation of wet-bulk density essentially matches the variation in water content (Fig. 25).

Wet-bulk density increases from 1.4 to 1.9 g/cm³, from near the seafloor to about 50 mbsf, and remains constant below that to the base of Hole 942A (Fig. 25). All whole-round sections from Holes 942A, 942B, and 942C were passed through the GRAPE, and the wet-bulk densities determined by the device are anomalously high.

The GRAPE data were determined to be unreliable after a malfunction of the GRAPE was identified.

Compressional-wave Velocity

Compressional-wave velocity measurements were made with the PWL and the DSV. Both instruments gave similar results (Fig. 26), although an offset occurs between Sections 942A-1H-1 and -2. Pervasive microfractures in sediment affected by gas expansion restricted PWL measurements to the interval from the top to 22.2 mbsf in Hole 942A. The average transverse velocities range between 1450 m/s and 1540 m/s. Longitudinal and transverse velocity were measured with the DSV from 1.05 through 17.11 mbsf. Longitudinal velocities range from 1493 to 1517 m/s, and transverse velocities range from 1496 to 1555 m/s, generally showing isotropic behavior (Table 12).

Shear Strength

Measurements of undrained shear strength were made using the motorized shear vane on all cores from Hole 942A (Table 13). Below 42 mbsf, compressive strengths were determined using a pocket penetrometer.

The strength profile for Hole 942A can be divided into two parts at approximately 40 mbsf (Fig. 27). Within the upper part, undrained shear strength increases relatively uniformly from 5 kPa just below the seafloor to 24 kPa at 39.49 mbsf. The increase in strength with depth below 40 mbsf is characterized by increased variability. A small increase of about 10 kPa occurs at the top of Unit VI. A prominent feature of the lower part of the strength profile is the pattern of strength increasing with depth within individual XCB cores. This pattern has been noted at previous sites (e.g., Site 937). As with the index properties, the changes in shear and compressive strengths have been attributed to expansion of the upper part and possible compression of the lower part of cores during coring. Only the measurement at the base of each XCB core falls on the trend extrapolated from the APC part of Unit VI.

The residual undrained shear strength also increases downhole (Table 13), but at a lower rate than the peak strength, resulting in a slight downhole decrease in the residual/peak undrained shear strength ratio (Fig. 27). In the XCB cores, residual shear strength values increase with depth in the cores.

Resistivity

Longitudinal and transverse resistivity were determined for cores from Hole 942A (Table 14). Longitudinal resistivity decreases below

Table 11. Index properties at Site 942.

Core, section, interval (cm)	Depth (mbsf)	Water content (%)	Wet-bulk density (g/cm ³)	Grain density (g/cm ³)	Dry-bulk density (g/cm ³)	Porosity (%)	Void ratio
155-942A-							
1H-1, 104-106	1.04	61.2	1.39	2.84	0.54	81.4	4.36
1H-2, 64-66	2.14	58.8	1.41	2.66	0.58	78.7	3.70
1H-3, 44-46	3.44	46.8	1.56	2.70	0.83	69.9	2.32
2H-1, 74-76	4.54	52.8	1.50	2.80	0.71	75.4	3.06
2H-2, 92-94	6.22	50.7	1.50	2.74	0.74	73.3	2.75
2H-3, 72-74	7.52	50.6	1.52	2.67	0.75	72.7	2.67
2H-4, 95-97	9.25	43.7	1.62	2.71	0.91	67.2	2.05
2H-5, 73-75	10.53	49.3	1.54	2.69	0.78	71.9	2.56
2H-6, 68-70	11.98	48.8	1.57	2.77	0.80	72.0	2.57
3H-1, 116-118	14.46	45.6	1.59	2.70	0.86	68.8	2.21
3H-2, 95-97	15.75	42.3	1.65	2.70	0.95	65.9	1.93
3H-3, 80-82	17.10	47.8	1.57	2.74	0.82	71.0	2.44
3H-4, 82-84	18.62	46.2	1.58	2.72	0.85	69.5	2.27
3H-5, 70-72	20.00	46.2	1.62	2.79	0.87	70.0	2.34
3H-6, 75-77	21.55	45.9	1.58	2.70	0.86	69.1	2.23
3H-7, 21-23	22.51	45.0	1.60	2.70	0.88	68.3	2.16
4H-1, 90-92	23.70	36.5	1.77	2.80	1.12	61.1	1.57
4H-2, 90-92	25.20	40.3	1.68	2.70	1.00	64.1	1.78
4H-3, 94-96	26.74	38.9	1.71	2.76	1.05	63.2	1.72
4H-4, 105-107	28.35	43.8	1.64	2.79	0.92	68.0	2.13
4H-5, 86-88	29.66	31.2	1.84	2.71	1.26	54.6	1.20
4H-6, 95-97	31.25	29.5	1.86	2.72	1.31	52.7	1.11
4H-7, 28-30	32.08	38.8	1.73	2.79	1.06	63.3	1.73
5H-1, 95-97	33.25	35.9	1.75	2.70	1.12	59.6	1.48
5H-2, 99-101	34.79	37.7	1.72	2.71	1.07	61.6	1.61
5H-3, 86-88	36.16	34.2	1.79	2.72	1.18	58.0	1.38
5H-4, 88-90	37.42	35.1	1.77	2.72	1.15	59.0	1.44
5H-5, 13-15	38.15	33.7	1.80	2.77	1.19	57.9	1.37
5H-6, 90-92	39.49	33.0	1.84	2.77	1.23	57.1	1.33
5H-7, 90-92	40.99	40.5	1.66	2.71	0.99	64.3	1.80
6H-1, 92-94	42.72	31.7	1.83	2.73	1.25	55.3	1.24
6H-2, 92-94	44.22	29.2	1.87	2.70	1.33	52.1	1.09
6H-3, 92-94	45.72	30.2	1.85	2.71	1.29	53.4	1.15
6H-4, 93-95	47.23	33.8	1.81	2.79	1.20	58.2	1.39
6H-5, 104-106	48.84	27.9	1.93	2.78	1.39	51.3	1.05
6H-6, 94-96	50.24	31.5	1.85	2.77	1.27	55.5	1.24
7H-1, 94-96	52.24	26.6	1.93	2.74	1.41	49.3	0.97
7H-2, 136-138	54.16	31.6	1.84	2.73	1.26	55.2	1.23
7H-3, 89-91	55.19	31.1	1.84	2.73	1.27	54.6	1.20
7H-4, 89-91	56.69	29.8	1.88	2.78	1.32	53.6	1.15
7H-5, 109-111	58.39	30.1	1.88	2.74	1.31	53.5	1.15
7H-6, 53-55	59.33	31.2	1.85	2.71	1.28	54.6	1.20
7H-7, 20-22	60.50	30.6	1.87	2.80	1.30	54.6	1.20
8H-1, 95-97	61.75	30.9	1.84	2.89	1.27	55.7	1.26
8H-2, 117-119	63.47	32.1	1.82	2.77	1.24	56.1	1.28
8H-3, 90-92	64.70	35.8	1.76	2.74	1.13	59.9	1.49
8H-5, 91-93	67.71	35.4	1.75	2.74	1.13	59.4	1.46
8H-6, 93-95	69.23	33.0	1.82	2.82	1.22	57.5	1.35
8H-7, 19-21	69.99	33.4	1.80	2.84	1.20	58.2	1.39
9H-1, 91-93	71.21	33.4	1.91	2.75	1.27	57.3	1.34
9H-2, 52-54	72.32	32.5	1.87	2.72	1.26	56.1	1.28
9H-4, 100-102	73.67	31.1	1.75	2.73	1.21	54.6	1.20
9H-7, 98-100	76.41	30.0	1.87	2.71	1.31	53.2	1.13
10H-1, 97-99	80.77	29.9	1.90	2.74	1.33	53.3	1.14
10H-2, 83-85	82.13	30.9	1.86	2.68	1.28	53.8	1.17
10H-3, 79-81	83.59	29.9	1.87	2.76	1.31	53.5	1.15
10H-4, 65-67	84.95	29.6	1.89	2.76	1.33	53.2	1.14
10H-5, 65-67	86.45	29.2	1.89	2.74	1.34	52.5	1.10
10H-6, 51-53	87.81	29.9	1.88	2.70	1.32	52.8	1.12
10H-7, 57-59	89.37	28.7	1.92	2.75	1.37	52.0	1.08
11H-1, 19-21	89.49	30.9	1.87	2.74	1.29	54.5	1.20
11H-2, 22-24	90.21	27.8	1.92	2.70	1.39	50.4	1.02
11H-3, 13-15	91.60	29.1	1.89	2.72	1.34	52.1	1.09
11H-4, 64-66	93.41	29.2	1.89	2.71	1.34	52.2	1.09
11H-5, 42-44	94.35	29.7	1.87	2.70	1.31	52.7	1.11
11H-6, 16-18	95.59	29.1	1.90	2.73	1.35	52.3	1.10
12H-1, 103-105	99.83	27.7	1.93	2.71	1.39	50.3	1.01
12H-2, 73-75	100.82	27.6	1.92	2.68	1.39	50.0	1.00
12H-3, 106-108	102.65	27.0	1.96	2.72	1.43	49.6	0.98
12H-4, 39-41	103.48	27.5	1.94	2.73	1.41	50.3	1.01
13X-1, 107-109	105.07	31.5	1.83	2.71	1.25	54.9	1.22
13X-2, 85-87	106.35	30.1	1.86	2.74	1.30	53.5	1.15
13X-3, 96-98	107.96	30.0	1.90	2.76	1.33	53.6	1.15
14X-1, 105-107	111.15	32.0	1.83	2.72	1.25	55.5	1.25
14X-2, 81-83	112.41	31.2	1.86	2.71	1.28	54.5	1.20
14X-3, 113-115	114.23	29.6	1.88	2.72	1.32	52.7	1.11
15X-1, 92-94	120.62	32.5	1.83	2.80	1.24	56.8	1.31
15X-2, 101-103	122.21	30.7	1.90	2.77	1.32	54.5	1.20
15X-3, 94-96	123.64	30.7	1.86	2.70	1.29	53.9	1.17
15X-4, 72-74	124.92	29.1	1.91	2.78	1.35	52.7	1.12
15X-5, 15-17	125.85	29.7	1.91	2.76	1.34	53.2	1.14
16X-1, 108-110	130.38	31.3	1.85	2.74	1.27	55.0	1.22
16X-2, 108-110	131.88	30.6	1.86	2.79	1.29	54.5	1.20
16X-3, 108-110	133.38	30.0	1.88	2.70	1.32	53.0	1.13
16X-4, 108-110	134.88	28.7	1.92	2.80	1.37	52.4	1.10
17X-1, 83-85	139.83	30.6	1.85	2.79	1.29	54.5	1.20
17X-2, 86-88	141.36	29.4	1.90	2.79	1.34	53.2	1.14

Table 11 (continued).

Core, section, interval (cm)	Depth (mbsf)	Water content (%)	Wet-bulk density (g/cm ³)	Grain density (g/cm ³)	Dry-bulk density (g/cm ³)	Porosity (%)	Void ratio
17X-3, 86-88	142.86	29.8	1.88	2.75	1.32	53.3	1.14
17X-4, 56-58	144.06	28.0	1.94	2.80	1.39	51.5	1.06
18X-1, 108-110	149.68	30.3	1.85	2.72	1.29	53.5	1.15
18X-2, 108-110	151.18	29.5	1.89	2.77	1.33	53.1	1.13
18X-3, 108-110	152.68	29.0	1.91	2.76	1.36	52.4	1.10
18X-4, 108-110	154.18	29.0	1.89	2.69	1.34	51.8	1.07
18X-5, 108-110	155.68	26.8	1.93	2.73	1.41	49.4	0.98
19X-1, 73-75	159.03	29.5	1.89	2.72	1.33	52.6	1.11
19X-2, 70-72	160.50	30.1	1.87	2.75	1.30	53.7	1.16
19X-3, 82-84	162.12	29.3	1.88	2.76	1.33	52.7	1.12
19X-4, 100-102	163.80	28.7	1.90	2.74	1.35	51.8	1.08
19X-5, 110-112	165.40	28.3	1.90	2.74	1.36	51.3	1.05
20X-1, 60-62	168.50	30.4	1.88	2.76	1.31	54.1	1.18
20X-2, 97-99	170.37	29.0	1.90	2.77	1.35	52.5	1.10
20X-CC, 13-15	170.97	28.2	1.95	2.80	1.40	51.8	1.07

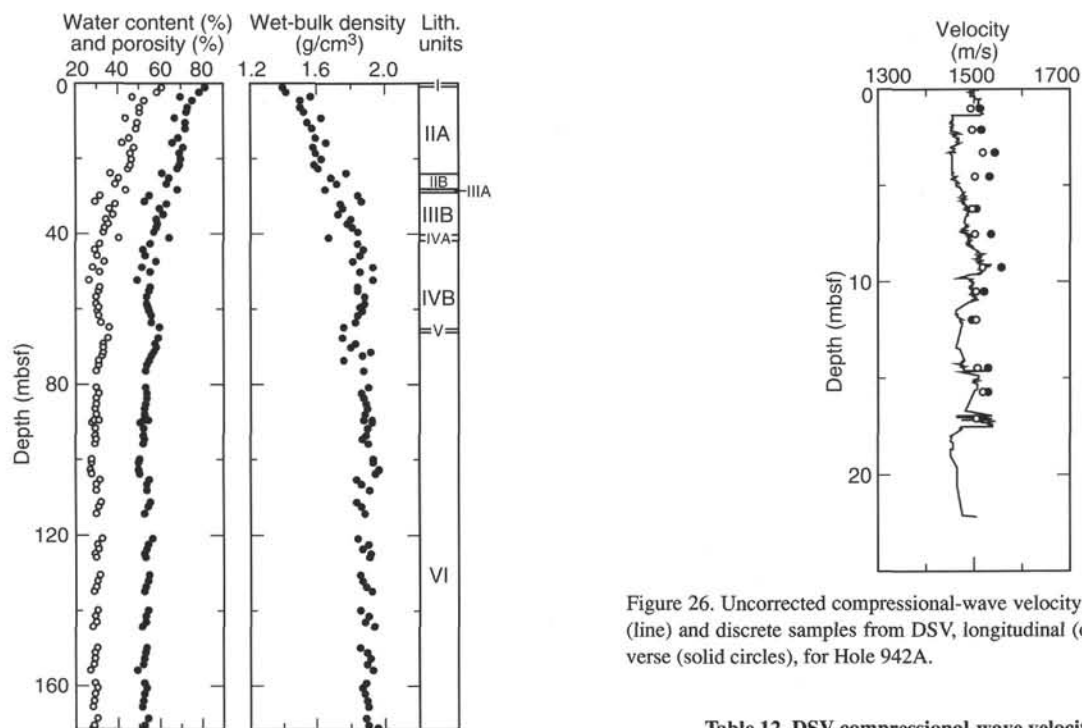


Figure 25. Water content (open circles) and porosity (solid circles), and wet-bulk density for Hole 942A.

seabed from 0.28 Ωm to 0.20 Ωm at about 7 mbsf and remains constant for the rest of Unit II. Through Unit III resistivity increases rapidly to 0.34 Ωm at 48 mbsf. Below 48 mbsf, resistivity remains near constant to the base of the hole, except for an increase of about 0.02 Ωm through the APC-cored section of lithologic Unit VI. Comparison of longitudinal and transverse resistivities indicates that the sediment is nearly isotropic. The resistivity anisotropy averages -1% over the length of the hole and displays no clear lithologic or down-hole trends (Fig. 28).

CORE-SEISMIC INTEGRATION

Site 942 is located on the crest of an abandoned levee at the westernmost edge of the Amazon Fan. The stratigraphic relationship of this channel-levee system to the other Amazon Fan channel-levee systems is uncertain because of the poor seismic control in this region of the fan. Four seismic-facies units are identified on a 3.5-kHz pro-

Figure 26. Uncorrected compressional-wave velocity determined from PWL (line) and discrete samples from DSV, longitudinal (open circles) and transverse (solid circles), for Hole 942A.

Table 12. DSV compressional-wave velocity at Site 942.

Core, section, interval (cm)	Depth (mbsf)	Longitudinal velocity (m/s)	Transverse velocity (m/s)
155-942A-			
1H-1, 101-109	1.05	1493	1511
1H-2, 61-69	2.15	1495	1514
1H-3, 31-39	3.35	1518	1543
2H-1, 71-79	4.55	1501	1531
2H-2, 89-97	6.23	1496	1504
2H-3, 69-77	7.53	1501	1534
2H-4, 92-100	9.26	1518	1555
2H-5, 70-78	10.54	1503	1519
2H-6, 65-73	11.99	1504	1496
3H-1, 113-121	14.47	1507	1528
3H-2, 92-100	15.76	1518	1528
3H-3, 77-85	17.11	1504	1514
3H-4, 81-89	18.65	1335	

file (1009UTC on 9 May 1994 during Leg 155; Figs. 3 and 29) and on *Farnella* and *Conrad* seismic profiles (Fig. 2). Seismic-facies Units 1 through 3 are classified using 3.5-kHz profiles, whereas Unit 4 is classified from the air-gun profiles (Fig. 30). The seismic facies could not be classified on the seismic profiles in the interval from 55 to 100 ms because reflections are obscured by the outgoing pulse, and

Table 13. Undrained shear strength at Site 942.

Core, section, interval (cm)	Depth (mbsf)	Peak undrained shear strength (kPa)	Residual undrained shear strength (kPa)	Unconfined compressive strength* (kPa)	Core, section, interval (cm)	Depth (mbsf)	Peak undrained shear strength (kPa)	Residual undrained shear strength (kPa)	Unconfined compressive strength* (kPa)
155-942A-					16X-4, 109	134.89	54.8	35.4	147.2
1H-1, 105	1.05	5.0	4.1		17X-1, 84	139.84	35.4	20.4	73.6
1H-2, 65	2.15	4.9	3.6		17X-2, 87	141.37	47.7	31.9	103.0
1H-3, 45	3.45	5.4	4.1		17X-3, 87	142.87	50.4	27.7	117.7
2H-1, 75	4.55	8.8	5.6		17X-4, 57	144.07	53.0	31.1	132.4
2H-2, 93	6.23	8.2	5.7		18X-1, 108	149.68	31.8	23.6	98.1
2H-3, 73	7.53	9.1	6.2		18X-2, 108	151.18	46.0	27.5	117.7
2H-4, 96	9.26	11.2	7.7		18X-3, 108	152.68	61.9	40.0	171.7
2H-5, 74	10.54	11.3	7.8		18X-4, 108	154.18	65.4	42.4	147.2
2H-6, 69	11.99	12.9	8.0		18X-5, 108	155.68	66.3	41.2	161.9
3H-1, 117	14.47	12.4	8.3		19X-1, 74	159.04	32.7	21.0	83.4
3H-2, 96	15.76	13.7	9.0		19X-2, 71	160.51	50.4	28.8	107.9
3H-3, 81	17.11	14.0	9.6		19X-3, 83	162.13	54.8	32.0	107.9
3H-4, 83	17.13	14.2	9.5		19X-4, 101	163.81	75.1	42.7	157.0
3H-5, 71	20.00	13.7	9.3		19X-5, 111	165.41	94.6	45.2	176.6
3H-6, 76	21.56	14.6	9.7		20X-1, 61	168.51	40.7		103.0
3H-7, 22	22.52	14.0	9.5		20X-2, 98	170.38	80.4	40.0	161.9
4H-1, 91	23.71	16.4	10.8		20X-CC, 8	170.98	68.1	32.0	196.2
4H-2, 91	25.21	17.8	11.7						
4H-3, 94	26.74	13.5	8.7						
4H-4, 106	28.36	18.3	11.7						
4H-5, 87	29.67	21.4	13.2						
4H-6, 96	31.26	22.1	13.3						
4H-7, 29	32.09	22.4	14.0						
5H-1, 96	33.26	24.3	15.6						
5H-2, 100	34.80	22.1	14.8						
5H-3, 87	36.17	20.9	14.2						
5H-4, 89	37.43	24.9	16.2						
5H-5, 13	38.17	22.6	15.2						
5H-6, 90	39.49	24.0	15.9						
5H-7, 90	40.99	29.7	18.1						
6H-1, 92	42.72	27.4	17.0	29.4					
6H-2, 92	44.22	22.6	16.5	39.2					
6H-3, 92	45.72	23.8	14.7	49.1					
6H-4, 92	47.22	28.3	16.7	54.0					
6H-5, 104	48.84	43.6	25.5	73.6					
6H-6, 93	50.23	21.5	15.1	49.1					
7H-1, 95	52.25	31.4	22.8	58.9					
7H-2, 137	54.17	26.7	19.9	49.1					
7H-3, 90	55.20	33.4	22.2	63.8					
7H-4, 90	56.70	37.0	24.4	68.7					
7H-5, 110	58.40	30.3	20.1	44.2					
7H-6, 53	59.33	59.33	22.1	16.3					
7H-7, 21	60.54			49.1					
8H-1, 95	61.75	23.1	14.0	49.1					
8H-2, 118	63.48	26.7	16.7	54.0					
8H-3, 91	64.71	36.0	19.2	68.7					
8H-5, 91	67.71	57.1	31.9	78.5					
8H-6, 94	69.24	37.0	23.1	83.4					
8H-7, 20	70.00	34.5	20.8	83.4					
9H-1, 91	71.21	40.6	26.2	73.6					
9H-2, 54	72.30	56.6	38.2	107.9					
9H-4, 100	73.70	37.1	25.1	93.2					
9H-5, 64	74.81	41.5	20.9	98.1					
9H-7, 100	76.43	41.5	20.4	83.4					
10H-1, 98	80.78	38.9	21.6	98.1					
10H-2, 83	82.13	38.0	15.9	73.6					
10H-3, 79	83.59	48.6	29.7	107.9					
10H-4, 68	84.98	50.4	27.9	98.1					
10H-5, 66	86.46	39.8	26.9	98.1					
10H-6, 52	87.82	38.9	19.6	93.2					
10H-7, 57	89.37	40.7	25.3	98.1					
11H-1, 20	89.50	32.7	23.8	68.7					
11H-2, 23	90.22	63.6	38.0	137.3					
11H-3, 12	91.61	39.8	25.9	98.1					
11H-4, 65	93.61	23.0	17.1	73.6					
11H-5, 43	94.36	30.1	20.3	93.2					
11H-6, 17	95.62	35.4	23.7	98.1					
12H-1, 104	99.84	49.5	22.2	98.1					
12H-2, 74	100.83	64.5	30.4	137.3					
12H-3, 107	102.66	46.9	20.5	107.9					
12H-4, 40	103.49	55.7	32.1	132.4					
13X-1, 108	105.08	26.5	18.0	44.2					
13X-2, 86	106.36	32.7	19.9	78.5					
13X-3, 97	107.97	52.2	31.5	103.0					
14X-1, 106	111.16	28.3	16.7	44.2					
14X-2, 82	112.42	37.1	25.0	63.8					
14X-3, 114	114.24	49.5	29.8	107.9					
15X-1, 93	120.63	27.4	14.0	63.8					
15X-2, 102	122.22	35.4	24.2	68.7					
15X-3, 95	123.65	41.5	23.6	98.1					
15X-4, 73	124.93	54.8	32.8	107.9					
15X-5, 16	125.86	47.7	30.0	112.8					
16X-1, 109	130.39	32.7	24.7	68.7					
16X-2, 109	131.89	30.1	21.4	73.6					
16X-3, 109	133.39	46.0	30.1	107.9					

Note: * = unconfined compressive strength (q_u) can be used to approximate undrained shear strength (S_u) by the relationship $q_u = 2S_u$.

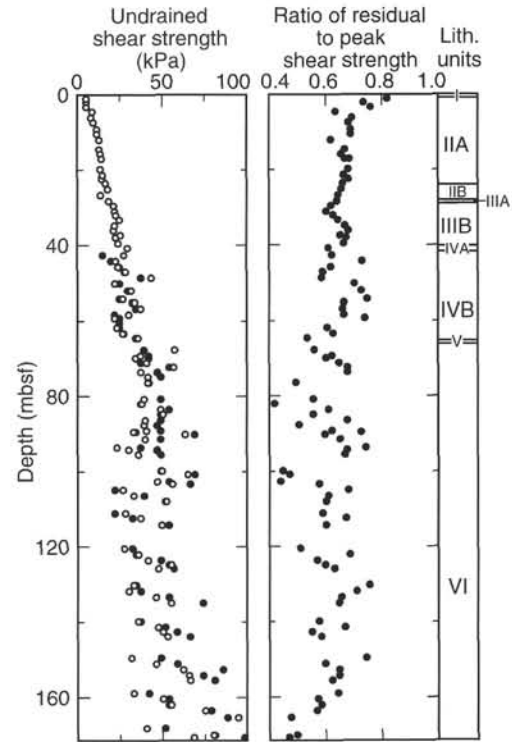


Figure 27. Undrained shear strength (open circles) and assumed undrained shear strength derived from unconfined compressive strength (solid circles). At right, ratio of residual to peak undrained shear strength.

this interval is below the depth of the acoustic penetration on 3.5-kHz records. Therefore, the base of seismic-facies Unit 3 and the top of seismic-facies Unit 4 are only approximate positions. Compression-wave velocities measured between 0 and 22 mbsf (Cores 942A-1H through -3H) were used to determine the thickness of the upper seismic units by integration. These results are comparable with the velocity-depth equation determined at Site 931.

Seismic-facies Unit 1 (0–13 ms) is characterized by continuous, parallel reflections that correlate to the Holocene nannofossil-fora-

Table 14. Electrical resistivity at Site 942.

Core, section, interval (cm)	Depth (mbsf)	Longitudinal resistivity (Ωm)	Transverse resistivity (Ωm)	Core, section, interval (cm)	Depth (mbsf)	Longitudinal resistivity (Ωm)	Transverse resistivity (Ωm)
155-942A-				7H-7, 21	60.51	0.341	0.319
1H-1, 105	1.05	0.282	0.263	8H-1, 95	61.75	0.335	0.337
1H-2, 65	2.15	0.249	0.235	8H-2, 117	63.47	0.336	0.335
1H-3, 45	3.45	0.231	0.234	8H-3, 91	64.71	0.337	0.330
2H-1, 75	4.55	0.240	0.237	8H-5, 91	67.71	0.326	0.306
2H-2, 93	6.23	0.215	0.212	8H-6, 94	69.24	0.314	0.323
2H-3, 73	7.53	0.204	0.213	8H-7, 20	70.00	0.319	0.312
2H-4, 37	8.67	0.219	0.220	9H-1, 92	71.22	0.334	0.318
2H-4, 96	9.26	0.223	0.223	9H-2, 54	72.34	0.333	0.318
2H-5, 74	10.54	0.224	0.223	9H-4, 94	73.61	0.342	0.335
2H-5, 127	11.07	0.245	0.237	9H-5, 63	74.80	0.360	0.339
2H-6, 69	11.99	0.215	0.215	9H-6, 100	76.09	0.354	0.359
3H-1, 117	14.47	0.227	0.225	10H-1, 97	80.77	0.361	0.410
3H-2, 24	15.04	0.223	0.228	10H-2, 83	82.13	0.367	0.365
3H-2, 96	15.76	0.229	0.227	10H-3, 80	83.60	0.353	0.353
3H-2, 142	16.22	0.225	0.219	10H-4, 68	84.98	0.366	0.370
3H-3, 22	16.52	0.226	0.226	10H-5, 65	86.45	0.368	0.377
3H-3, 141	17.71	0.234	0.234	10H-6, 50	87.80	0.364	0.379
3H-4, 22	18.02	0.232	0.236	10H-7, 57	89.37	0.365	0.359
3H-4, 83	18.63	0.227	0.221	11H-1, 20	89.50	0.339	0.324
3H-4, 133	19.13	0.253	0.262	11H-2, 23	90.22	0.366	0.351
3H-5, 10	19.40	0.209	0.194	11H-3, 12	91.61	0.352	0.331
3H-5, 71	20.01	0.214	0.224	11H-4, 65	93.42	0.380	0.407
3H-5, 130	20.60	0.213	0.216	11H-5, 43	94.36	0.377	0.355
3H-6, 16	20.96	0.213	0.200	11H-6, 17	95.60	0.353	0.352
3H-6, 76	21.56	0.214	0.202	12H-1, 104	99.84	0.369	0.361
3H-6, 128	22.08	0.216	0.226	12H-2, 74	100.83	0.369	0.360
3H-7, 22	22.52	0.232	0.213	12H-3, 107	102.66	0.382	0.393
3H-7, 42	22.72	0.196	0.197	12H-4, 40	103.49	0.370	0.371
4H-1, 91	23.71	0.248	0.215	13X-1, 108	105.08	0.319	0.303
4H-1, 140	24.20	0.217	0.218	13X-2, 86	106.36	0.331	0.332
4H-2, 91	25.21	0.184	0.200	13X-3, 97	107.97	0.333	0.330
4H-2, 129	25.59	0.217	0.231	14X-1, 106	111.16	0.325	0.308
4H-3, 94	26.74	0.212	0.213	14X-2, 82	112.42	0.321	0.317
4H-3, 124	27.04	0.207	0.208	14X-3, 114	114.24	0.348	0.329
4H-4, 106	28.36	0.187	0.195	15X-1, 93	120.63	0.303	0.299
4H-4, 144	28.74	0.190	0.205	15X-2, 102	122.22	0.334	0.323
4H-5, 87	29.67	0.249	0.247	15X-3, 95	123.65	0.327	0.320
4H-5, 143	30.23	0.233	0.238	15X-4, 73	124.93	0.355	0.338
4H-6, 96	31.26	0.262	0.234	15X-5, 16	125.86	0.354	0.339
4H-6, 135	31.65	0.253	0.291	16X-1, 109	130.39	0.342	0.325
4H-7, 29	32.09	0.216	0.213	16X-2, 109	131.89	0.332	0.322
4H-7, 71	32.51	0.230	0.227	16X-3, 109	133.39	0.368	0.324
5H-1, 94	33.24	0.240	0.245	16X-4, 109	134.89	0.330	0.354
5H-2, 100	34.80	0.260	0.260	17X-1, 84	139.84	0.334	0.320
5H-3, 87	36.17	0.282	0.275	17X-2, 87	141.37	0.346	0.324
5H-4, 86	37.40	0.278	0.272	17X-3, 87	142.87	0.342	0.325
5H-5, 13	38.17	0.293	0.276	17X-4, 57	144.07	0.361	0.339
5H-6, 90	39.49	0.299	0.290	18X-1, 108	149.68	0.323	0.345
5H-7, 90	40.99	0.257	0.274	18X-2, 108	151.18	0.341	0.339
6H-1, 92	42.72	0.315	0.338	18X-3, 108	152.68	0.341	0.349
6H-2, 92	44.22	0.308	0.312	18X-4, 108	154.18	0.343	0.356
6H-3, 92	45.72	0.331	0.325	18X-5, 108	155.68	0.337	0.385
6H-4, 93	47.23	0.305	0.311	19X-1, 74	159.04	0.331	0.313
6H-5, 104	48.84	0.346	0.343	19X-2, 71	160.51	0.328	0.329
6H-6, 93	50.23	0.346	0.335	19X-3, 83	162.13	0.340	0.344
7H-1, 95	52.25	0.342	0.345	19X-4, 101	163.81	0.358	0.336
7H-2, 137	54.17	0.328	0.331	19X-5, 111	165.41	0.353	0.356
7H-3, 90	55.20	0.322	0.329	20X-1, 61	168.51	0.327	0.336
7H-4, 90	56.70	0.335	0.328	20X-2, 98	170.38	0.360	0.339
7H-5, 110	58.40	0.355	0.342	20X-CC, 8	170.98	0.354	0.357
7H-6, 53	59.33	0.339	0.362				

minifer clay of lithologic Unit I, and the top 8 m of the bioturbated mud of Subunit IIA. Seismic-facies Unit 2 (13–20 ms) is acoustically transparent. This unit correlates with the middle position of lithologic Subunit IIA and appears to correspond to the thicker debris-flow deposit to the south of the site (Fig. 29). However, the lithology of the cores through this unit shows no evidence for a debris-flow deposit. The prominent reflector at the interface of seismic-facies Units 2 and 3 correlates to a sand layer found at 14 mbsf within Subunit IIA. Seismic-facies Unit 3 consists of moderate-amplitude, continuous, slightly converging reflections between 20 and 55 ms. This seismic-facies unit correlates to the lower portion of lithologic Subunit IIA and all of Subunits IIB, IIIA, and IIIB, which are predominantly interbedded muds with silt/sand laminae and beds. The prominent reflector at 25 ms corresponds to the first occurrence of silt laminae at 18 mbsf. Another prominent reflector at 32 ms correlates to the interface between lithologic Subunits IIA and IIB, where there is an increase in frequen-

cy and thickness of silt and sand beds. The reflection at the base of seismic-facies Unit 3 correlates to the contact between lithologic Subunits IIB and IVA at 41 mbsf. This boundary marks the top contact of a foraminifer-nannofossil-rich clay unit. A similar lithologic unit, Subunit VA at 65 mbsf, presumably marks the uppermost boundary of a buried channel-levee system cored at this site (Figs. 2 and 30). Seismic-facies Unit 4 (100–220 ms) is acoustically transparent and correlates with the overbank deposits of the buried channel-levee system.

IN-SITU TEMPERATURE MEASUREMENTS

Temperature gradients and heat flow were determined using two downhole measurements and the bottom-water (mud-line) temperature. Two ADARA measurements were made during Cores 942A-6H

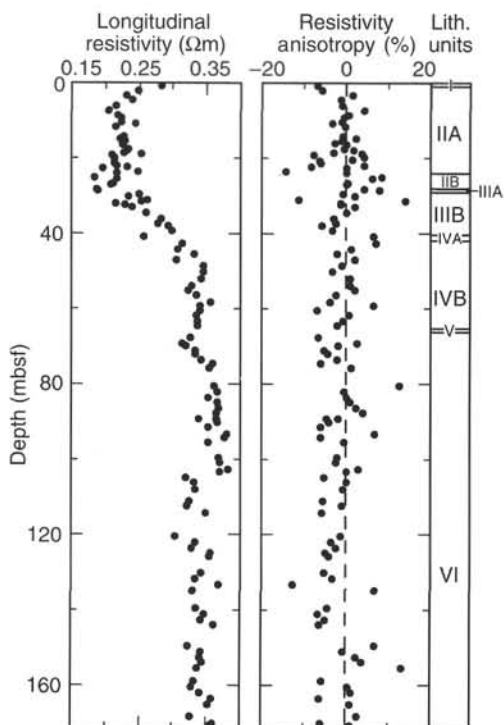


Figure 28. Longitudinal resistivity and resistivity anisotropy for Hole 942A.

(51 mbsf) and -9H (80 mbsf) using instrument number 12. The mud-line temperature of 2.59°C measured from this instrument was used as the reference bottom-seawater temperature at Site 942. Successful measurements resulted in extrapolated equilibrium temperatures of 4.46°C at 51 mbsf, and 5.66°C at 80 mbsf.

Equilibrium temperatures, extrapolated from synthetic curves constructed to fit transient temperature data, are plotted as a function of depth (mbsf) in Figure 31. Using the ADARA mud-line temperature and the sub-bottom temperatures from the two ADARA measurements downhole, the geothermal temperature gradient can be approximated by a linear mean of 38.2°C/km. We calculated heat flow by adopting the constant geothermal temperature gradient of 38.2°C/km and a linear increase in the thermal conductivity, K , of 1.1 ± 0.15 W/(m·K), which is an average of regression estimates at 80 mbsf. This results in a calculated heat flow of 42 mW/m².

SYNTHESIS AND SIGNIFICANCE

Stratigraphic Synthesis

Surficial Nannofossil-Foraminifer Clay (Unit I)

Unit I (0–0.66 mbsf) is an intensely bioturbated Holocene nannofossil-foraminifer clay, with an iron-rich diagenetic crust at the base of the unit.

Last-glacial Mud and Silt (Unit II)

Unit II (0.66–28.10 mbsf) consists of mud with interbedded laminae and beds of silt and very fine sand. The mud has 1.4%–4.5% carbonate content. The unit is subdivided into two subunits. Subunit IIA (0.66–23.85 mbsf) comprises bioturbated mud with hydroxylite-stained mottles and includes one sand bed at 14 mbsf. Rare laminae and thin beds of silt occur below 17 mbsf. Subunit IIB (23.85–28.10 mbsf) is composed of mud with thin to thick beds of silt and fine

sand, that increase in frequency and thickness toward the base of the subunit.

Last-interglacial Mud, Sand, and Calcareous Clay (Units III–V)

Unit III (28.10–40.18 mbsf) comprises a thin bed of calcareous mud (0.70 m) resting on a sequence of mud with interbedded silt and sand. Subunit IIIA (28.10–28.80 mbsf) is a foraminifer-nannofossil-rich silty clay with 14% carbonate and has a gradational contact with the underlying Subunit IIIB (28.80–40.18 mbsf), which consists of color-mottled bioturbated mud with interbedded laminae and beds of silt and sand. Silt and sand beds are particularly abundant from 36 to 40 mbsf. *Spreiten* burrows (probably *Echinocardium*) commonly disrupt the tops of sand beds.

Unit IV (40.18–65.20 mbsf) resembles Unit III, comprising a thin bed (0.62 m) of calcareous mud resting on a sequence of mud with interbedded silt and sand. Sand is more abundant than in Unit III. Subunit IVA (40.18–40.80 mbsf) is a foraminifer-nannofossil-rich clay similar to that in Subunit IIIA and with a gradational lower boundary. Subunit IVB (40.80–65.20 mbsf) consists of moderately burrowed, dark greenish gray mud, alternating with beds and laminae of very fine sand and coarse silt, many of which are cross laminated.

Unit V (65.20–66.07 mbsf) consists of greenish gray foraminifer-nannofossil clay with as much as 31% carbonate and gradational boundaries with the under- and overlying units.

Mud and Silt at the Top of a (?) Middle-levée-complex Levee (Unit VI)

Unit VI (66.07–171.28 mbsf) consists of gray mud with laminae and rare beds of silt. Color banding and mottling are common. Carbonate content is generally 0.7%–4%. Two light-colored muds with 14%–17% carbonate contain diagenetic siderite. Some samples at the top of Unit VI have anomalously high grain density (2.8–2.9 g/cm³); a similar property was observed at the base of Unit IV.

Implications

Foraminifers and nannofossils are common to abundant in Units I–V and the upper part of Unit VI, but are rare in the lower part of Unit VI. The *P. obliquiloculata* 40-ka datum occurs at 23 mbsf and the Ericson X/Y Zone boundary (85 ka) is between 33 and 42 mbsf. Because *G. tumida* is absent below 70.38 mbsf, this lower interval is interpreted as the W Zone (isotopic Stage 6, >130 ka).

Two geomagnetic excursions were identified from short intervals of anomalous remanence direction and intensity. The Lake Mungo Excursion (30 ka) occurs at 11.5 mbsf in Hole 942A (also observed in Hole 942C, but not detected in Hole 942B). The Blake Event (105 ka) is found at 41.5 mbsf in Hole 942B (also found in Hole 942C; see also Cisowski, this volume). Short wavelength (about 0.5 m) oscillations in magnetic inclination, interpreted as secular variation, were detected between 1 and 12 mbsf; similar fluctuations were detected deeper in the holes. Remanence intensity variation can be correlated between holes.

This site provides a reference section for biostratigraphy and stable isotopes on the western side of the Amazon Fan. The three carbonate-rich intervals (Subunits IIIA, IVA, and Unit V) are interpreted to correspond to isotopic Stages 5a, 5c, and 5e, with the Blake paleomagnetic event in Stage 5c and the greatest abundance of microfossils when sea level was highest in Stage 5e. The stratigraphy of Site 942 will serve as a standard against which to interpret the carbonate-rich intervals of Sites 931, 933, 935, 936, 944, and 946 and thus provide a biostratigraphic framework for the entire fan. The overall sedimentation rate in Stage 5 is estimated to be 0.8 m/k.y., compared with 0.4 m/k.y. in Stages 2–4. The difference can be accounted for by the abundant sand turbidites in Stage 5.

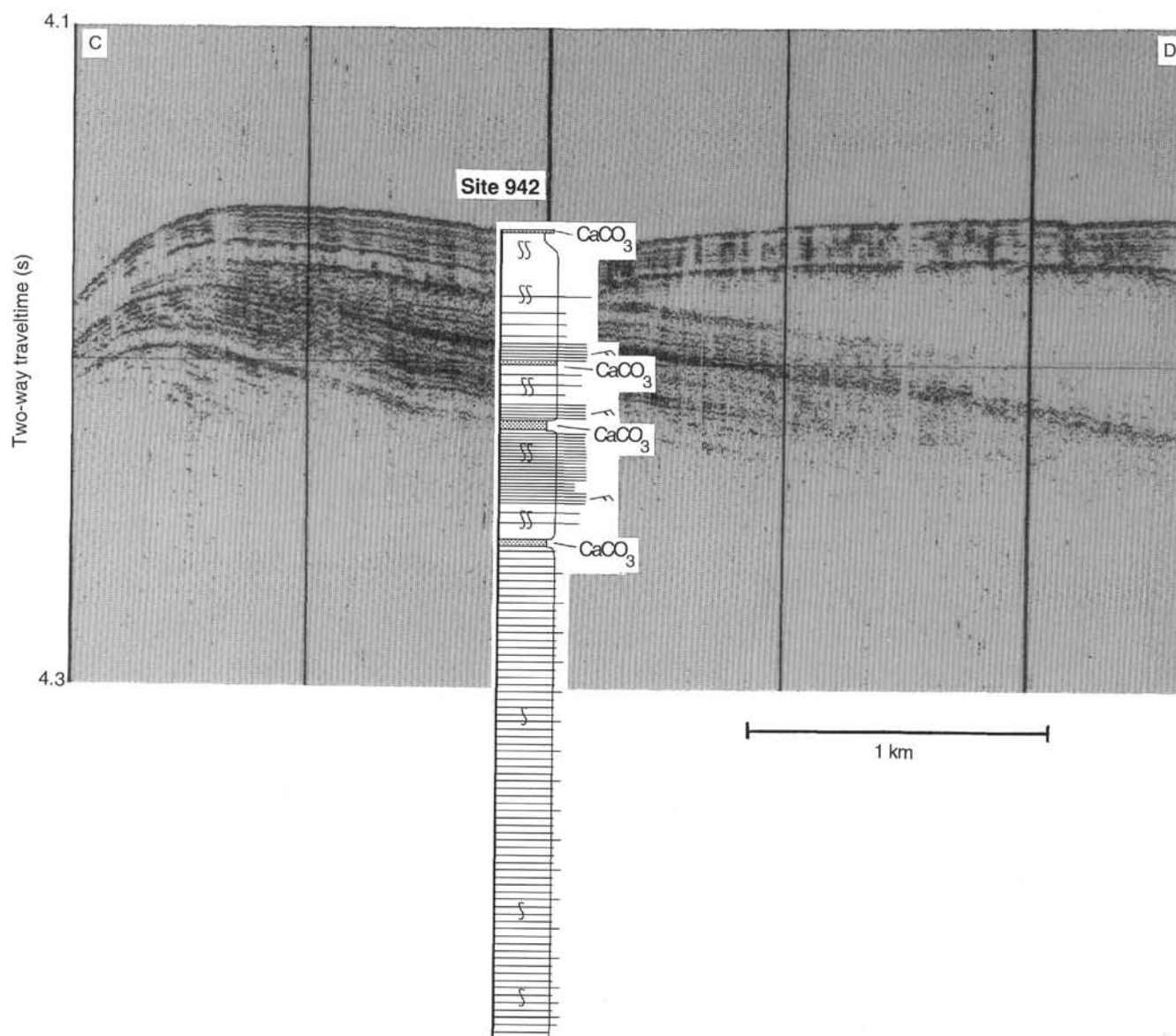


Figure 29. 3.5-kHz seismic reflection profile at Site 942 with the corresponding lithostratigraphic section (location shown in Fig. 4). Carbonate-rich zones are identified by CaCO_3 .

The turbidites at Site 942 are different from those at other Leg 155 sites. The 7- to 50-cm-thick isolated sand bed at 14 mbsf may be correlated acoustically (seismic-facies Unit II; Fig. 32) with the edge of a debris flow that has ponded against the levee crest (Fig. 3) and is interpreted to be extensive from GLORIA data (Fig. 4). Sediment near this interval in the core does not appear to have been disturbed by the debris flow. The sand bed is the only indication of the debris flow observed in the sediment record. The less-reflective interval above the sand layer in 3.5-kHz profiles may result from deposition on an irregular sand bed, rather than from the deposition of a debris-flow unit at this site.

The 3.5-kHz profile (Fig. 2) shows that the lower part of lithologic Subunit IIA through Subunit IIIB thickens away from the levee crest. Turbidites in Subunits IIB to IVB (interpreted as isotopic Stages 3–5) contain a high proportion of fine sand to silt. Ripple-migration directions, determined on oriented cores, are to the north. This direction is down the regional slope but toward the axis of the sinuous channel just north of the drill site (Fig. 4). Where not bioturbated, ripple cross-lamination passes up into laminated sediment of the Bouma T_d division, indicating that the ripples were formed by turbidity currents.

The abundance of ripple lamination at this site reflects the abundance of very fine sand, in which current ripples form over a wide range of flow velocities based on flume data. The sand may have been eroded from outer shelf sands as sea level fell. This sand may have been sorted and deposited during the preceding transgression, which is recorded by calcareous clays in deep water. Given the probable lowering of sea level by <30 m during Stage 5 (see “Introduction” chapter, this volume), erosion must have taken place in many tens of meters water depth at the shelf break, probably under the influence of storm waves.

The silty turbidites of Unit VI (interpreted as isotopic Stage 6), in contrast, lack sand. They resemble other Amazon Fan levee sediment types in their grain size distribution, organic carbon and carbonate content, and color. The sediment formed during the early and most active growth phase of the levee was probably not penetrated at this site.

Total organic carbon content generally decreases downhole from Unit I to Unit V, from 0.8% to 0.4%, but varies with lithology. Total organic carbon then gradually increases from 0.8% to 1.0% through Unit VI. Total nitrogen shows a distribution pattern similar to that of carbon. Elevated sulfur content occurs immediately below Units I

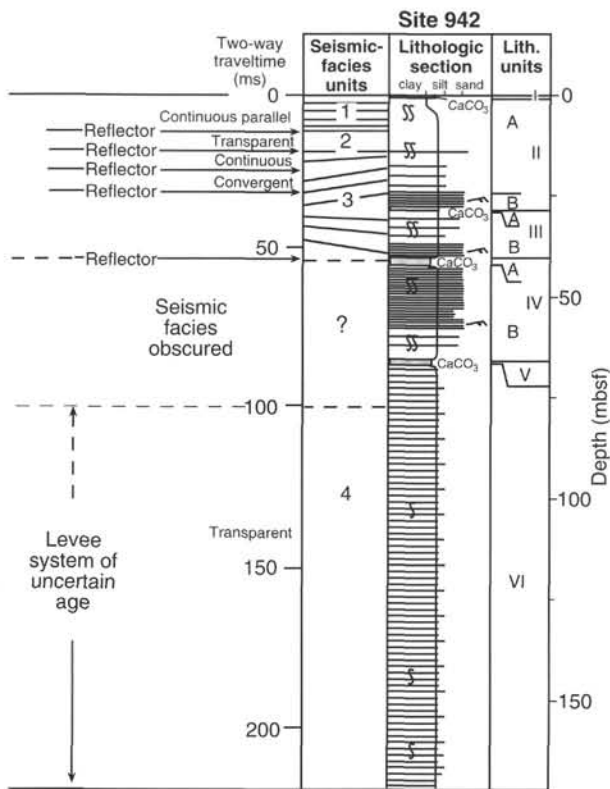


Figure 30. Correlation of lithostratigraphic observations with seismic-facies units and prominent reflections at Site 942.

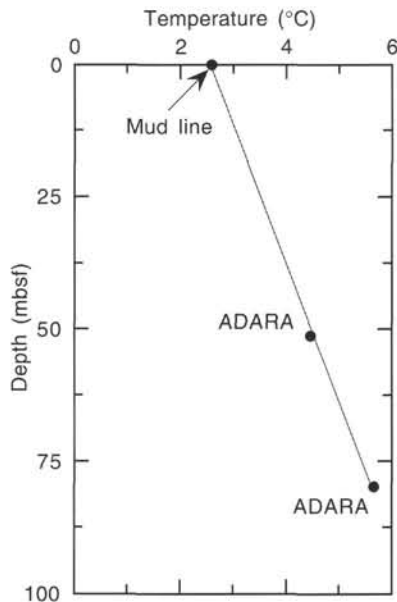


Figure 31. Estimated equilibrium temperatures in Hole 942A. A linear curve fit through the data suggests that reliable equilibrium temperatures were acquired that indicate a geothermal gradient of 38.18°C/km.

and V, but otherwise shows a progressive downhole decrease from 1.3% to about 0.5% through Units I–V and is generally low (0.5%–0.8%) through Unit VI. Pore-water calcium, magnesium, alkalinity, and salinity are low in the interval 30–90 mbsf, corresponding to the interval of low organic carbon, thereby suggesting a role for remineralization of organic carbon in evolution of pore water. The high organic carbon in Unit VI resembles that found in other Amazon Fan levee sediment types. The organic carbon in Units I–V is less abundant and has a [C/N]_a ratio suggesting the importance of a marine source.

REFERENCES*

Allen, J.R.L., 1984. *Sedimentary Structures: Their Character and Physical Basis*: Amsterdam (Elsevier).
 Bouma, A.H., 1962. *Sedimentology of Some Flysch Deposits: A Graphic Approach to Facies Interpretation*: Amsterdam (Elsevier).
 Damuth, J.E., 1977. Late Quaternary sedimentation in the western equatorial Atlantic. *Geol. Soc. Am. Bull.*, 88:695–710.
 Damuth, J.E., and Embley, R.W., 1981. Mass-transport processes on the Amazon Cone: western equatorial Atlantic. *AAPG Bull.*, 65:629–643.
 Damuth, J.E., Flood, R.D., Kowsmann, R.O., Belderson, R.H., and Gorini, M.A., 1988. Anatomy and growth pattern of Amazon deep-sea fan as revealed by long-range side-scan sonar (GLORIA) and high-resolution seismic studies. *AAPG Bull.*, 72:885–911.
 Milliman, J.D., Summerhayes, C.P., and Barretto, H.T., 1975. Quaternary sedimentation on the Amazon continental margin: a model. *Geol. Soc. Am. Bull.*, 86:610–614.
 Nittrouer, C.A., Kuehl, S.A., DeMaster, D.J., and Kowsmann, R.O., 1986. The deltaic nature of Amazon shelf sedimentation. *Geol. Soc. Am. Bull.*, 97:444–458.

*Abbreviations for names of organizations and publications in ODP reference lists follow the style given in *Chemical Abstracts Service Source Index* (published by American Chemical Society).

Ms 155IR-118

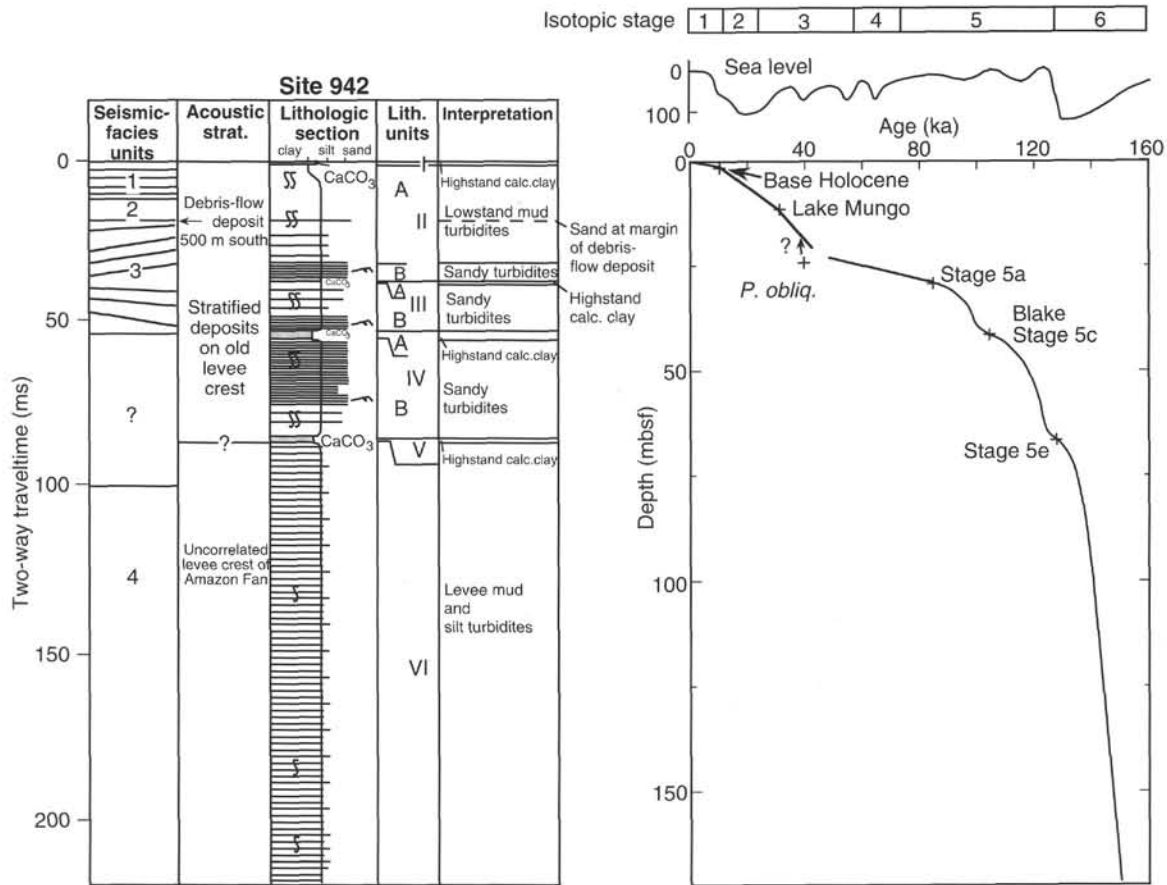


Figure 32. Summary of Site 942 showing (left to right) seismic-facies units, acoustic stratigraphy, schematic lithologic column, lithologic units, interpreted sediment facies, chronological picks, and interpreted age-depth curve (+ = datums; variations in slope between these points are interpreted, based on dated intervals of similar facies at other sites).

NOTE: For all sites drilled, core-description forms (“barrel sheets”) and core photographs can be found in Section 4, beginning on page 703. Forms containing smear-slide data can be found in Section 5, beginning on page 1199. GRAPE, index property, magnetic susceptibility, and natural gamma data are presented on CD-ROM (back pocket).